AN ABSTRACT OF THE THESIS OF

Srinivasan Subhash Sundaram for the degree of Master of Science in Electrical and Computer Engineering presented on June 14, 2017.

Title: Development of an Integrated Generator Power Take-off Strategy using Model Predictive Control (MPC) for Ocean Wave Energy Conversion

Abstract approved: _____

Ted K.A Brekken

Model Predictive Control (MPC) has previously been investigated on ocean wave energy converters (WEC) to improve the amount of power captured, while respecting the system constraints. Previous research done in the same area, focused on building a control scheme by using the knowledge of the past & current states of the system and predicting the future states of the system based on which the control action was taken for the power-take-off (PTO) to maximize power capture. This was done by maximizing the product of force and velocity and at the same time, staying under the permissible limits of both force and velocity (constraints). Our research attempts investigate if an integrated approach for power maximization is possible by trying to modify the way power maximization is done. This is made possible by integrating a state-space generator model with a state-space WEC model. This combined generator-WEC model is then used with an MPC

controller. So rather than having PTO-force as the input for the wave energy converter, dq reference frame voltages are used as inputs and the product of voltages and currents for the d and q axes (i.e. the electrical power) is maximized.

Development of an Integrated Generator Power Take-off Strategy using Model Predictive Control (MPC) for Ocean Wave Energy Conversion

by

Srinivasan Subhash Sundaram

A THESIS

submitted to

Oregon State University

in partial fulfillment of
the requirements for the
degree of

Master of Science

Presented June 14, 2017
Commencement June 2018

Master of Science thesis of Srinivasan Subhash Sundaram presented on June 14, 2017.

APPROVED:

Major Professor, representing Electrical and Computer Engineering

---

Director of the School of Electrical Engineering and Computer Science

---

Dean of the Graduate School

I understand that my thesis will become part of the permanent collection of Oregon State University libraries. My signature below authorizes release of my thesis to any reader upon request.

Srinivasan Subhash Sundaram, Author

ACKNOWLEDGEMENTS

I would like to thank my advisor Dr. Brekken for giving me the opportunity to work with him and for his immense help, guidance,enthusiasm, patience and expertise. Thank you Alan McCall and Pat McCleer for giving me the chance to work with Dehlsen . Also a huge thank you to my committee members Dr. Janet Tate, Dr. Eduardo Sanchez and Dr. Roberto Albertani for agreeing to be on my committee at such short notice.

I would also like to thank each and every member of the Energy systems group both past and present. Thank you Elliott, Phylicia, Nak, Brandon, Ziwei, Chen, Peng, Vishvas, Alex, Ridwan and Ian. I couldn't have asked for a much better set of friends/colleagues. Special thanks to Dr. Ratanak So who was always there to answer my questions.

Finally, I would like to thank my parents for all their love and support. I couldn't have been here without you guys.

TABLE OF CONTENTS

TABLE OF CONTENTS (Continued)

LIST OF FIGURES

LIST OF FIGURES (Continued)

Chapter 1: Introduction

1.1 Overview of different renewable energy sources

As defined by the EIA (Energy Information Administration), renewable or non-conventional energy sources are those which are available naturally. In other words, these are naturally replenished over the course of time. Tidal, wind, solar, geothermal and biomass are a few examples of renewable energy sources [1]. The future for power is clean energy since factors like global warming puts an emphasis on protecting the environment and this automatically increases the importance of how energy is being generated currently. Fig 1.1 glosses over the fact that renewables account for 10% of the total energy consumption by energy sources as of 2015.

Fig 1.1 also indicates that the energy consumption by source is about 22% for hydroelectric. This is expected to grow in the coming decades. Given that the demand for energy is constantly rising, it would be extremely beneficial for the energy sector to move towards green energy rather than relying on fossil fuels.

1.2 Why wave energy?

Among the various energy sources, wave energy is crucial especially in Oregon owing to its closeness to the coastline. Oregon is one of the few states that has pledged to make its electricity 50 percent renewables dependent [3], makes the

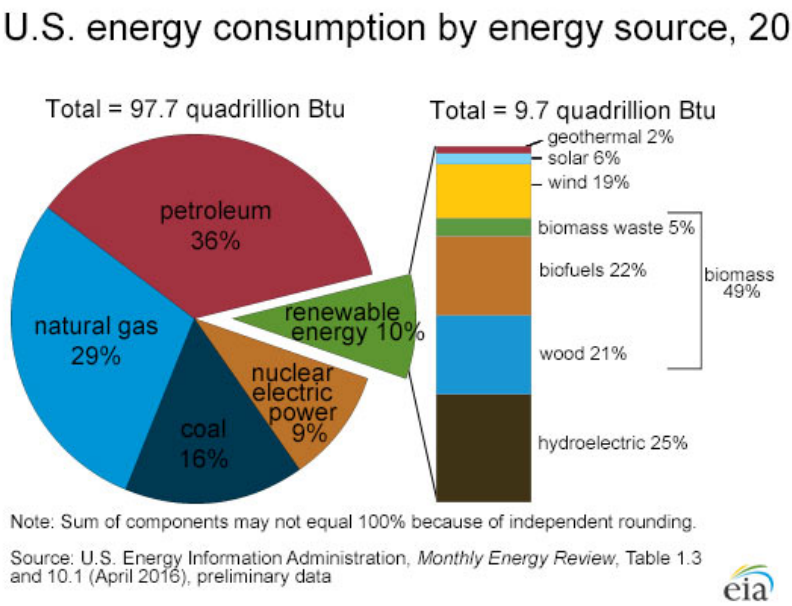

Figure 1.1: US energy consumption by energy sources (Image from [2]).

development of power generation technologies from wave energy important. In addition, the density of water is much higher compared to air. So there is potential for more energy to be exploited there. An interesting fact about wave energy is that the US receives 2100 terraWatts of incident waves along its coastline each year [4]. Harnessing a quarter of that would eclipse the total production of the US hydro system [4]. Additionally, wave energy is emission free compared to coal and natural gas which have detrimental effects on the environment. Apart from this, there are some well defined benefits of using wave energy namely :

- Predictability : Forecasting with precision is very much possible for waves unlike solar and wind [5]. Solar energy is not available at night and the velocity of wind varies with time. From a utility's point of view, this pre-

dictability of wave energy helps them to adjust their supply according to the demand and availability [5].

- Consistency : Water covers about 70% of the earth and it is available through the whole year [5].
- Proximity : Roughly 60% of the world's population live about 60 kilometers from the coast line [6]. This is important as it saves on transmission costs especially when it comes to wave energy [6].

1.3 Different WEC topologies

The earliest interest in harnessing the potential of wave energy can be traced back to the 1800s [7]. Over the past few centuries, there has been a steady growth in development of different wave energy conversion topologies and these can broadly be classified into three main categories namely [7] :

- Oscillating water column
- Overtopping
- Oscillating body

In the upcoming sub-sections, each topology is briefly discussed.

1.3.1 Oscillating water column

The OWC consists of an enclosed chamber that is inverted over water as shown in figure 1.2. This enclosure enables the water inside the chamber to compress and decompress thereby utilizing the heaving motion of the water [7]. There is a small opening in the chamber out of which the air rushes out as a result of compression and decompression of air inside the enclosure and this is used to rotate a turbine that serves as a medium of conversion for the energy [7]. The reason why a Wells turbine is preferred is because it spins in one direction regardless of direction of air flow.

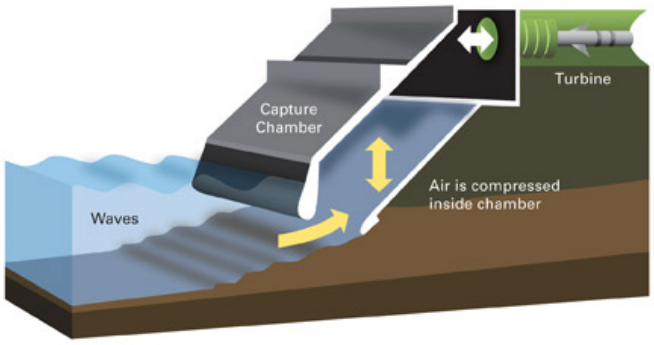

Figure 1.2: Oscillating water column showing movement of air (Image from [2])

1.3.2 Overtopping

Overtopping devices usually consist of a mechanism that captures the incident waves, sends them up a ramp where there is a reservoir to collect the incident waves. Once the collection is done, the water is usually drained out through a turbine outlet. Usually, low head turbines are used for the energy conversion[8].

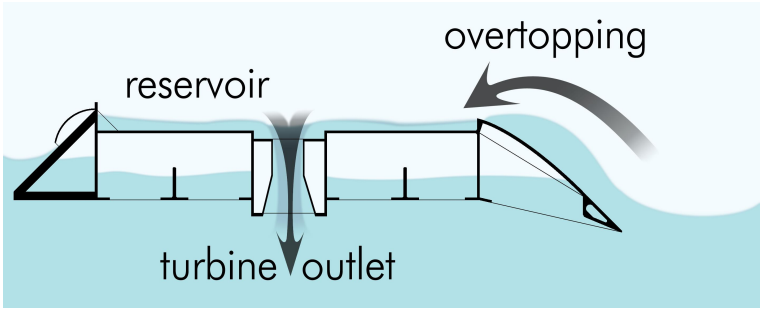

Figure 1.3: Working of the wave dragon (Image from [9]) .

1.3.3 Oscillating body

These devices are usually large scale WEC-devices that make use of one or two degrees of freedom with some form of power-take-off mechanism to convert mechanical energy to electrical energy. Usually point absorbers oscillate with the ocean wave in more than one degrees of freedom [10]. Also these devices are capable of energy absorption from waves that are much larger than the dimensions of the device itself thereby making them more robust [10]. The power take-off can be hydraulic or direct drive. Different power take-off methods are discussed in the upcoming chapters. A good example for an oscillating body is a point absorber

shown in the below figure. The working principle for a point absorber can be related to that of a simple Faraday flashlight. It makes use of the heave motion of the waves as that is where maximum energy capture is possible [11].

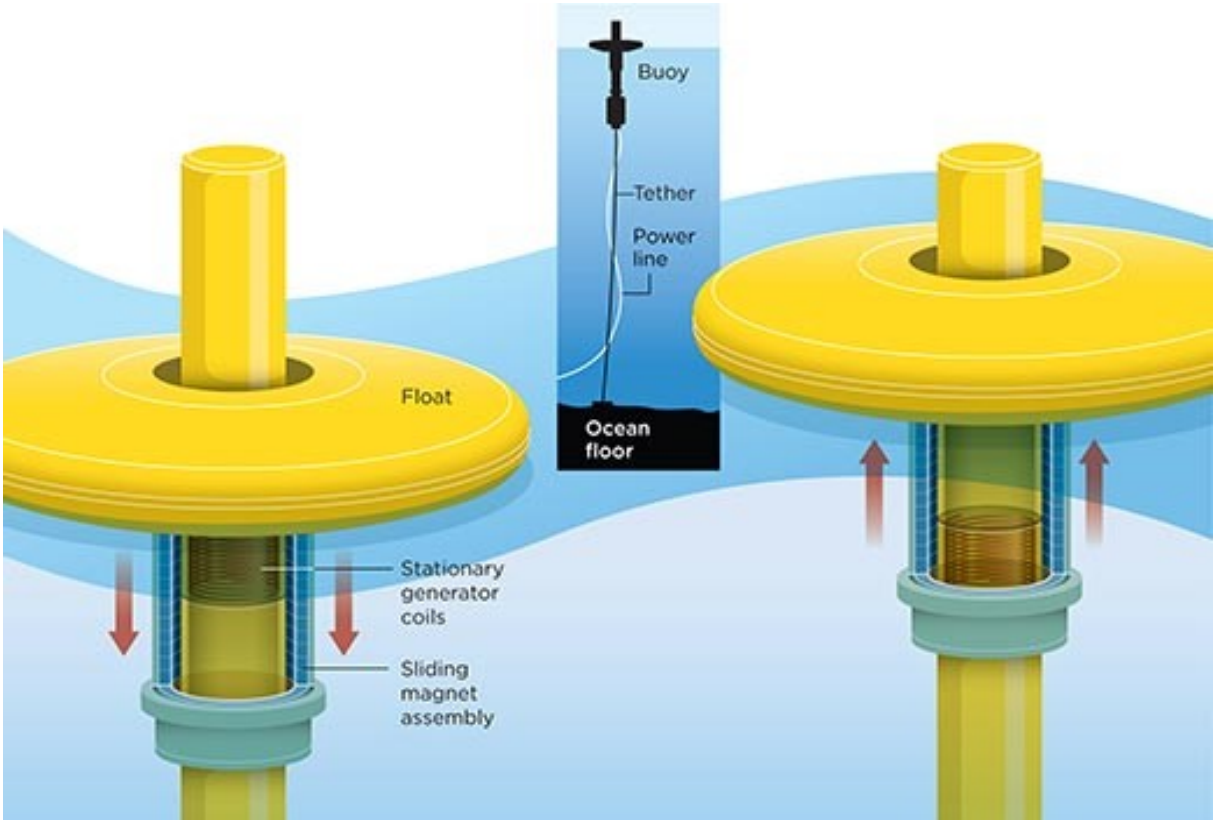

Figure 1.4: Point absorber (Image from [12]) .

1.4 Power take-off

Power take-off is defined as the mechanism to convert all the mechanical energy a device takes in from the ocean into electrical energy [13]. Power take off is directly linked to efficiency as higher the conversion rate is for captured power, higher the efficiency is[13]. Furthermore, adding power take-off mechanism also impacts the mass and the dynamics of the WEC [13]. Since PTO is part of the WEC, its construction must be robust and it be able to withstand harsh wave conditions i.e. maintenance costs for the PTO must be minimal [13]. Another interesting aspect of power take-off is that there is no set industry standard device for wave energy [13]. This leaves room for experimentation and the PTO mechanism chosen could be highly efficient or could be an impractical model. So, careful validation is required when it comes to choosing the right take-off mechanism for the converter. Fig 1.5 shows different ways in which wave energy can be converted to mechanical energy.

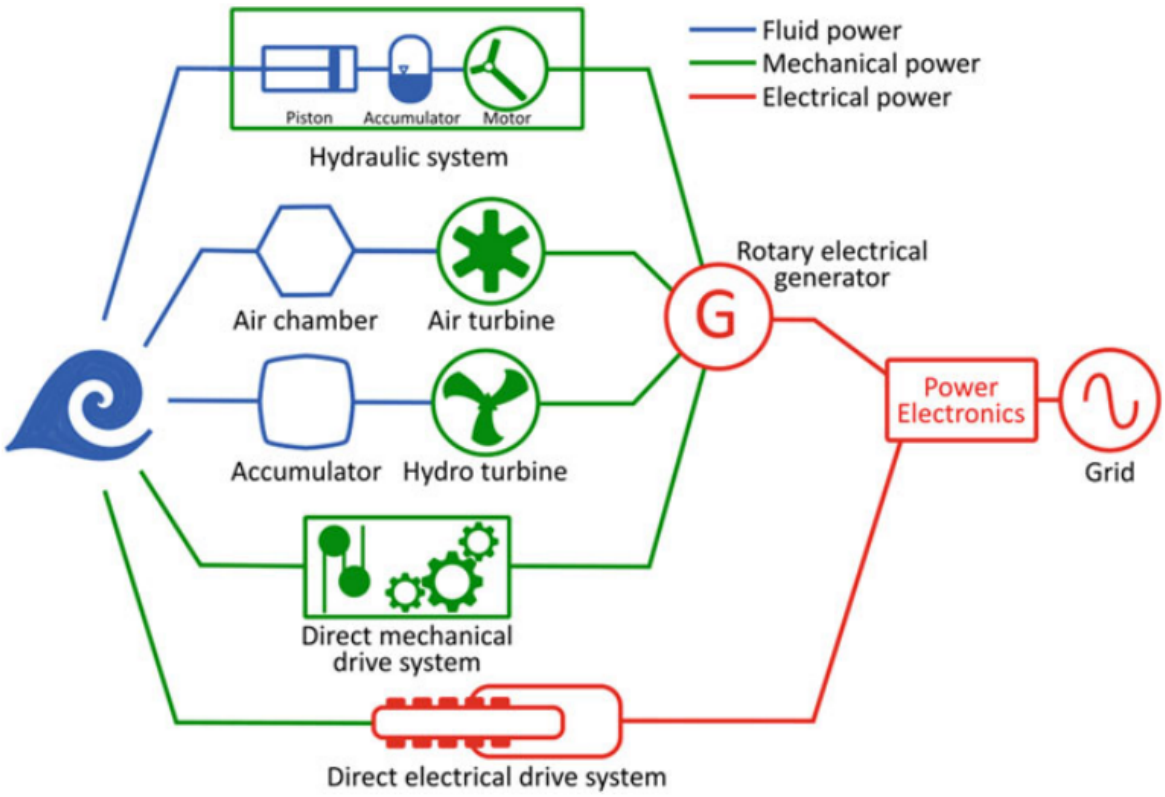

Figure 1.5: Different energy conversion paths (Image from [13]).

1.4.1 Turbines

As discussed before in the oscillating water column section, turbines (more typically a Wells turbine or impulse) is used as the power take-off mechanism. This mechanism has its drawbacks because even though its construction is simple, the Wells turbine is not self starting [13]. To overcome this, an impulse turbine is used which does compensate for the lack of starting and has low operational speeds,

but has many movable parts which makes its construction and maintenance a bit more complex [13].

1.4.2 Hydraulic power take-off

This mechanism is mostly used with point absorbers since waves operate at low speeds generating tremendous forces and point absorbers are ideal to capture this [14]. Fig 1.6 shows a typical hydraulic PTO where the movement of the buoy forces a rod to compress and decompress, thereby forcing fluid through the valves in a controlled manner to drive the electric generator [14]. Accumulators are also added to make sure the pressure is controlled [14].

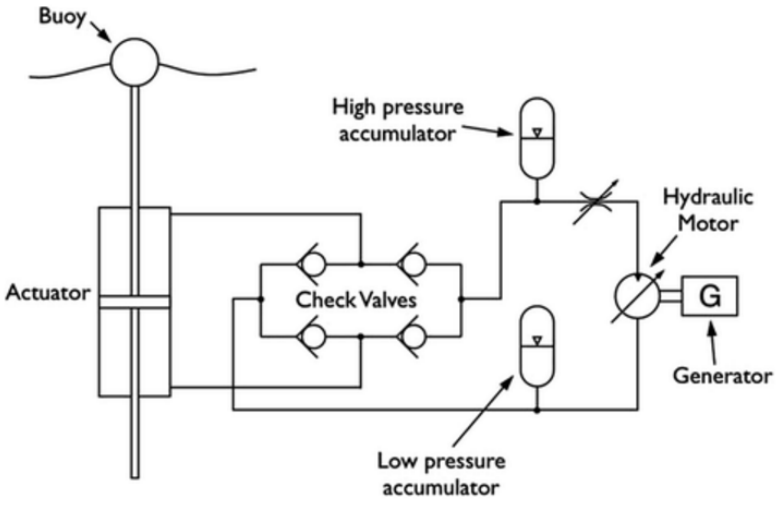

Figure 1.6: Schematic for hydraulic PTO (Image from [14]).

1.4.3 Direct-drive power take-off

As the name suggests, direct drive power take-off systems involves coupling a generator with the buoy i.e. there is no intermediate step in the conversion although rectification is done following the conversion [14].

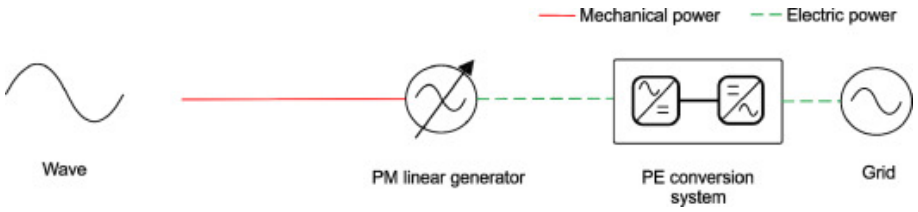

Figure 1.7: Conversion flow for DD PTO (Image from [15]).

With the technological advancements in the field of power electronics and permanent magnet machines, direct drive PTOs seem to be a very attractive prospect [14]. The one important aspect is that very precise construction is required to maintain the gaps between the translator and stator. Fig 1.8 shows a rough arrangement of the stator and the magnets with respect to the translator [14].

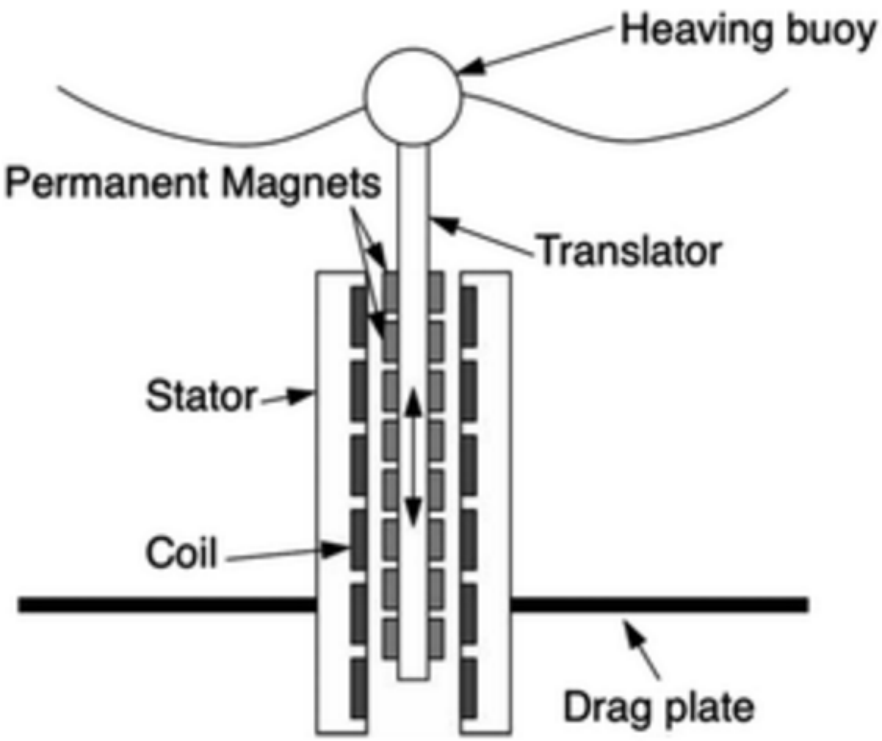

Figure 1.8: Schematic for DD PTO (Image from [14])

1.5 Different types of control schemes WECs

Although there are various control strategies, in this section, two control schemes are briefly discusses namely :

- Latching control
- Reactive control

1.5.1 Latching control

Introduced first by Falnes, latching control (say for a point absorber) deals with restricting the buoy when the velocity is zero and releasing it such that it is in phase with the waves [14]. This allows maximum power capture by the device [14]. Usually the buoy is stopped (latched) and released at the point where the buoy is in phase with the excitation force exerted by the waves [14]. This form of control usually requires some form power take off (say a hydraulic PTO) to push the buoy such that phase matching occurs [13]. This requires precise modelling of the controller to account for the desired degree(s) of freedom depending on the device type and wave type (regular or irregular) and predicting the excitation forces which usually becomes difficult in case of irregular waves [13]. The antithesis for latching is called declutching where the buoy is allowed to moved freely and power take-off is engaged only at desired velocities [14].

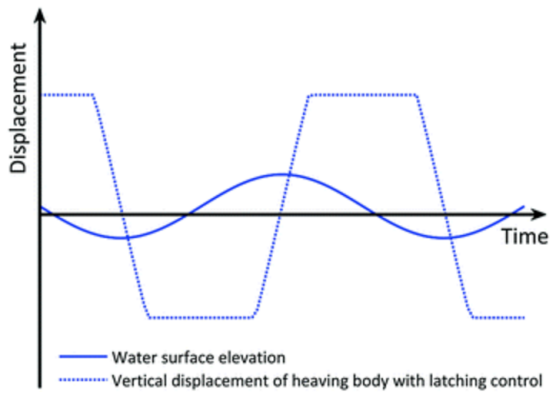

Figure 1.9: Latching mechanism for a buoy. (Image from [13]).

1.5.2 Reactive control

The basic idea of reactive power control is to put some power back into the ocean for a small duration of time at certain oscillating frequencies, [16] thereby widening the efficiency bands on either side of the resonant period [17]. A wave energy converter is often imagined as a spring damper system i.e. the spring/converter is pushed down and it comes back up again and continues to oscillate until it returns to its original position [13]. Various other components like inertia, spring constant, stiffness are also taken into consideration [17]. Ideally, maximum power extraction occurs when the buoy resonates at resonant frequency and this adjustment of the device is done by some form of power take-off and tuning the spring coefficients [16]. In simpler terms, this is the mechanical equivalent of impedance matching i.e. maximum power transfer occurs when the source impedance is equal to the load impedance [18].

1.6 Model predictive control & its usage in wave energy conversion

In any field of engineering be it chemical, mechanical or electrical, controls plays a significant role as depending on how good the control scheme is, profits are that much higher. In wave energy, controls become even more crucial because it directly impacts the efficiency. An ill-defined controller will not optimize power efficiently and might cause significant losses and increase the cost of power produced. Therefore, it is crucial to have a smoothly running controller that complements the plant. Depending on the type of wave energy converter being used and the method of

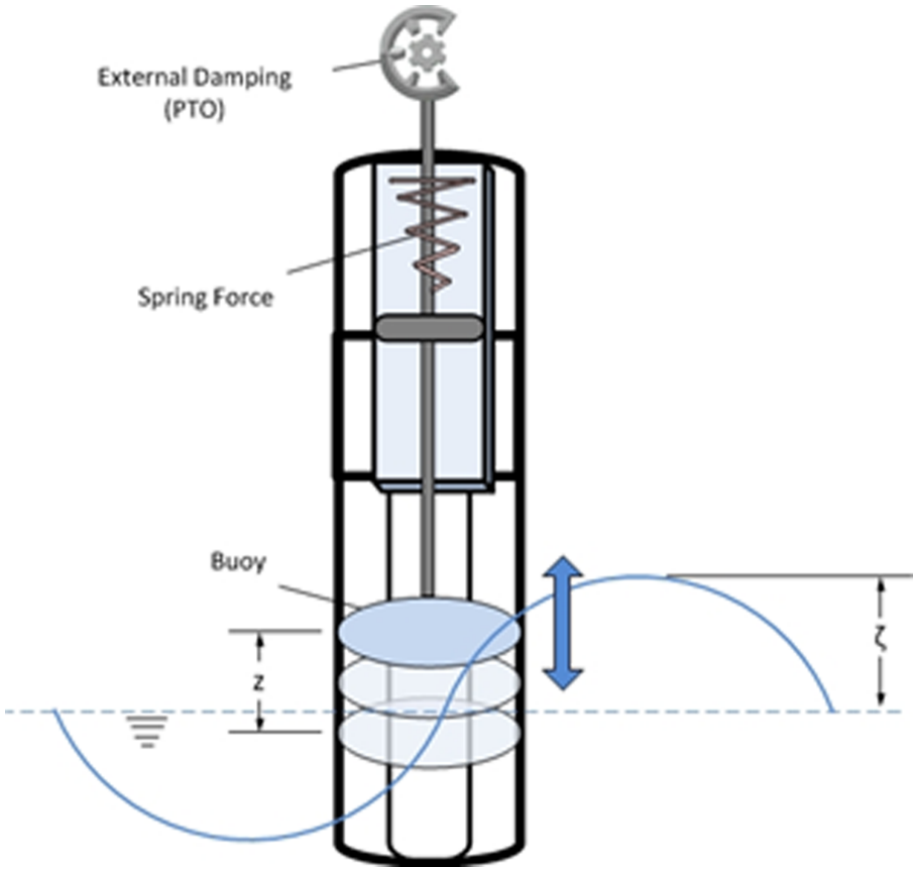

Figure 1.10: Buoy modeled as a spring damper. (Image from [19]).

power take-off chosen, complexity of the controller varies. The previous section talked briefly about latching and reactive control. However, over the past several years, optimization control techniques have been developed for WECs. Eidsmoen [20] developed the mathematical model for a heaving buoy to get the optimal velocity back in 1996. In more recent times,research in the field of model predictive control has gained traction because it works well with slow moving systems (where system response time is in the order of seconds) that have the capacity to produce

high energy and waves are perfect for this. This was demonstrated in the works done by [21],[22], [23]. The essence of model predictive control lies in extracting maximum power from the converter while respecting the system constraints. The detailed formulation for MPC is discussed in the upcoming sections.

1.7 Proposed idea

Over the past few years, studies done on advance control schemes using the optimization prowess of Model Predictive control, have shown that an improvement of 500 percent in power capture is possible when MPC is used instead of fixed damping (simulation-wise) [24]. The previous work done by [25],[24] dealt with treating the power take-off force as a product of force and velocity used a reactive control strategy that was previously discussed in the earlier sections to occasionally deliver power into the ocean in return for better alignment between converter force and velocity thereby optimizing the product of force and velocity. The current formulation attempts to take the research further by bringing an actual generator into the picture and try combining this hydrodynamic WEC model with a generator model to optimize the product of voltage times current i.e. the electrical power as opposed to mechanical power. There are however several questions that need to be addressed.

- Will the problem be convex?
- Will combining the generator model into the MPC formulation be feasible?

- How will this impact the efficiency of the system?
- How will this impact the overall stability of the system?

Detailed formulation of the MPC model and the results are discussed in the upcoming chapters.

Chapter 2: Plant model development

2.1 Structure for a control system model

Control system models are usually of two types

- Open loop system
- Closed loop system

The main difference between open and closed loop systems is that in closed loop systems, there is feedback from the states i.e. some knowledge of the system states is fed back to the input via feedback to adjust for stability. The process to model state space systems relies on writing the equations in state space representation as shown in equation 2.1 and 2.2. Closed loop control systems are much more effective in capturing the dynamics of the system and these are shown in the form of first order differential equations coupled with a set of variables that are termed as state variables [26].

$$\dot{x} = Ax + B_u u + B_v v \tag{2.1}$$

$$y = Cx + D_u u + D_v v \tag{2.2}$$

Dot notation is used to represent the set of first order differential equations w.r.t. time. The state vector x is a column vector of length n, the input vector u, is a column vector of length r. $\boldsymbol{A}$ is an nxn square matrix that represents weights for the system dynamics and $\boldsymbol{B}$ is a matrix of dimensions nxr that represents weights for the inputs [26]. Same notation goes for the output set of equations denoted by y. $\boldsymbol{C}$ is an mxn matrix and $\boldsymbol{D}$ is an mxr matrix which in some cases is a null matrix [26]. However, in the real world, $\boldsymbol{C}$ indicates usage of sensors and it is impractical to have one for every state.

For the formulations used in this research, the control system is divided into two portions as shown in Fig 2.1

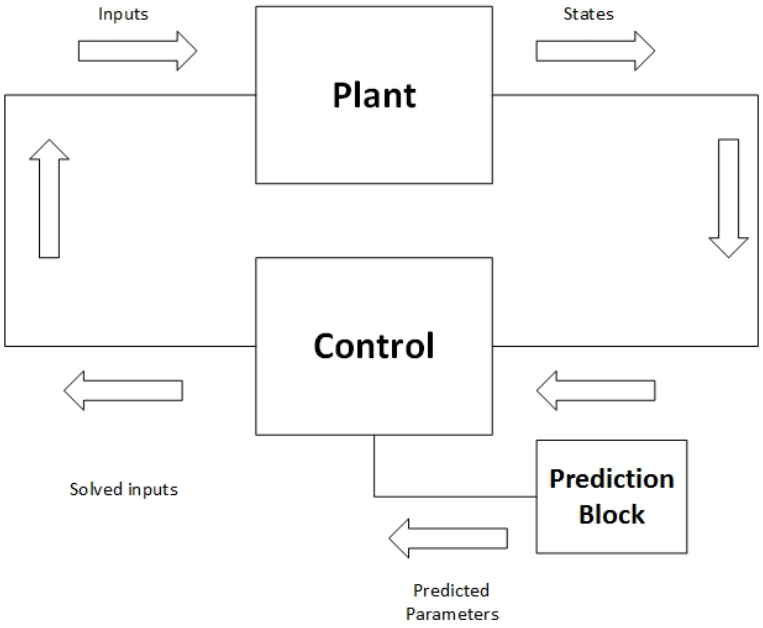

Figure 2.1: Control system block diagram

Additionally, the control model also has some form of prediction for the excitation force and the controller solves for inputs to be applied to the system that results in optimal power.

2.2 Hydrodynamic model from previous research

The efficiency of the control model depends on how well the plant model is defined. Recent research done in the field of advanced controls focused on building a fast and accurate state-space representation of a wave energy converter model (in particular

for multiple body wave energy converter) that serves as a an efficient hydrodynamic plant model for mathematical modelling in MATLAB [25]. It is important to note that in this formulation, the point absorber operates under linear wave theory conditions [7] i.e. we assume it is acted upon only in the heave direction by the waves since that is where maximum energy capture occurs.

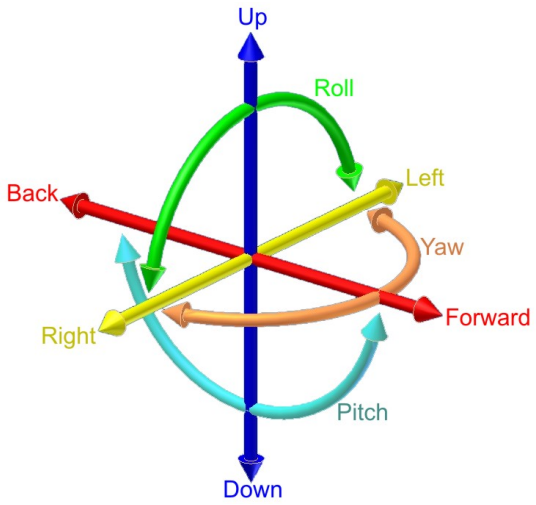

Figure 2.2: Six degrees of freedom [27]

Fig 2.2 shows the six degrees of freedom and the point absorber captures the heave direction i.e. the up and down motion of the buoy. After using these assumptions, the equations of motion were set up as per Falnes convention [28].

$$F_e(s) + F_r(s) + F_b(s) + F_{pto}(s) = sV(s)m \tag{2.3}$$

Here, F_e is the excitation force which is the force exerted by the waves, F_b is the buoyancy force, F_r is the radiation force caused by the movement of the device

and F_{pto} is the power take-off force which is the force applied by the machine on the device [28]. Following the modelling of WECs which was done in [25], initially, a frequency independent approximation is used for the buoy position and buoy velocity. Later on, the frequency dependency is augmented to build the model [25].

$$\frac{d}{dt}\begin{bmatrix}\dot{z}\\ z\end{bmatrix} = \underbrace{\begin{bmatrix}\frac{-B}{m+A} & \frac{-k}{m+A}\\ 1 & 0\end{bmatrix}}_{A}\begin{bmatrix}\dot{z}\\ z\end{bmatrix} + \underbrace{\begin{bmatrix}\frac{1}{m+A}\\ 0\end{bmatrix}}_{Bu}\begin{bmatrix}F_{pto}\end{bmatrix} + \underbrace{\begin{bmatrix}\frac{1}{m+A}\\ 0\end{bmatrix}}_{Bv}\begin{bmatrix}F_e\end{bmatrix} \tag{2.4}$$

The frequency dependency in the model comes from the radiation force formulation, the details of which are discussed in [25].

The resultant radiation force approximation after removing dependencies of F_r' as per [25] is :

$$\ddot{F}_r'(t) + \frac{c_{bb}}{c_{ba}}\dot{F}_r'(t) + \frac{c_{bc}}{c_{ba}}F_r'(t) = -\frac{c_{aa}}{c_{ba}}\,\ddot{z}(t) - \frac{c_{ab}}{c_{ba}}\,\dot{z}(t) \tag{2.5}$$

$$F_r(t) = F_r'(t) - A(\infty)\ddot{z}(t) \tag{2.6}$$

The equation of motion is then reduced to account for dependencies is discussed in [25]

$$F_e + F_r + F_b + F_{pto} = m\ddot{z} \tag{2.7}$$

$$F_r = F_r' - A(\infty)\ddot{z} \tag{2.8}$$

$$F_b = -k\ z \tag{2.9}$$

$$\ddot{F}_r' = -\frac{c_{bb}}{c_{ba}}\dot{F}_r' - \frac{c_{bc}}{c_{ba}}F_r' - \frac{c_{aa}}{c_{ba}}\ \ddot{z} - \frac{c_{ab}}{c_{ba}}\ \dot{z} \tag{2.10}$$

$$\ddot{z} = \frac{1}{m + A(\infty)}(F_e + F_r' + F_b + F_{pto}) \tag{2.11}$$

Removing time dependency, the final hydrodynamic equation as per [25]

$$\dot{F}_r' = -\frac{c_{bb}}{c_{ba}}F_r' - \frac{c_{bc}}{c_{ba}}\int_{-\infty}^{t} F_r'\ dt - \frac{c_{aa}}{c_{ba}}\ \dot{z} - \frac{c_{ab}}{c_{ba}}\ z \tag{2.12}$$

$$\frac{d}{dt}\begin{bmatrix} \dot{z} \\ z \\ F_r' \\ \int_{-\infty}^{t} F_r'\, d\tau \end{bmatrix} = \begin{bmatrix} 0 & \frac{-k}{m+A(\infty)} & \frac{1}{m+A(\infty)} & 0 \\ 1 & 0 & 0 & 0 \\ -\frac{c_{aa}}{c_{ba}} & -\frac{c_{ab}}{c_{ba}} & -\frac{c_{bb}}{c_{ba}} & -\frac{c_{bc}}{c_{ba}} \\ 0 & 0 & 1 & 0 \end{bmatrix} \begin{bmatrix} \dot{z} \\ z \\ F_r' \\ \int_{-\infty}^{t} F_r'\, d\tau \end{bmatrix} + \begin{bmatrix} \frac{1}{m+A(\infty)} \\ 0 \\ 0 \\ 0 \end{bmatrix} \begin{bmatrix} F_{pto} \end{bmatrix} + \begin{bmatrix} \frac{1}{m+A(\infty)} \\ 0 \\ 0 \\ 0 \end{bmatrix} \begin{bmatrix} F_e \end{bmatrix} \quad (2.13)$$

This hydrodynamic state-space representation of the buoy is now integrated with a generator model. The integration portion is discussed in the upcoming sections.

2.3 Generator models

In this section, two generator models that were chosen for integration. One being a simple dq machine model i.e. an AC generator model and the other being a simpler DC generator model. There are also various methods to formulate the model which are discussed in detail in the upcoming sections.

2.3.1 AC generator modelling

For a three phase machine (say a PM machine), we have as per [29]

$$v_A = Ri_A + \frac{\partial \lambda_A}{\partial t} \tag{2.14}$$

where rate of change of flux linkages is the sum of flux linkages between all the windings and the rotor magnets [29]

$$\frac{\partial \lambda_A}{\partial t} = \frac{\partial(\lambda_{AA} + \lambda_{AB} + \lambda_{AC} + \lambda_{fA}(\theta))}{\partial t} \tag{2.15}$$

Similarly for the other two windings, we have [29]

$$v_B = Ri_B + \frac{\partial \lambda_B}{\partial t} \tag{2.16}$$

where rate of change of flux linkages is [29]

$$\frac{\partial \lambda_B}{\partial t} = \frac{\partial(\lambda_{BA} + \lambda_{BB} + \lambda_{BC} + \lambda_{fB}(\theta))}{\partial t} \tag{2.17}$$

$$v_C = Ri_C + \frac{\partial \lambda_C}{\partial t} \tag{2.18}$$

where rate of change of flux linkages is [29]

$$\frac{\partial \lambda_C}{\partial t} = \frac{\partial(\lambda_{CA} + \lambda_{CB} + \lambda_{CC} + \lambda_{fC}(\theta))}{\partial t} \tag{2.19}$$

As the windings are interconnected, converting them to dq and solving them is the best option [29]

$$v_d = Ri_d + \frac{\partial \lambda_d}{\partial t} - \omega_d \lambda_q \tag{2.20}$$

$$v_q = Ri_q + \frac{\partial \lambda_q}{\partial t} + \omega_d \lambda_d \tag{2.21}$$

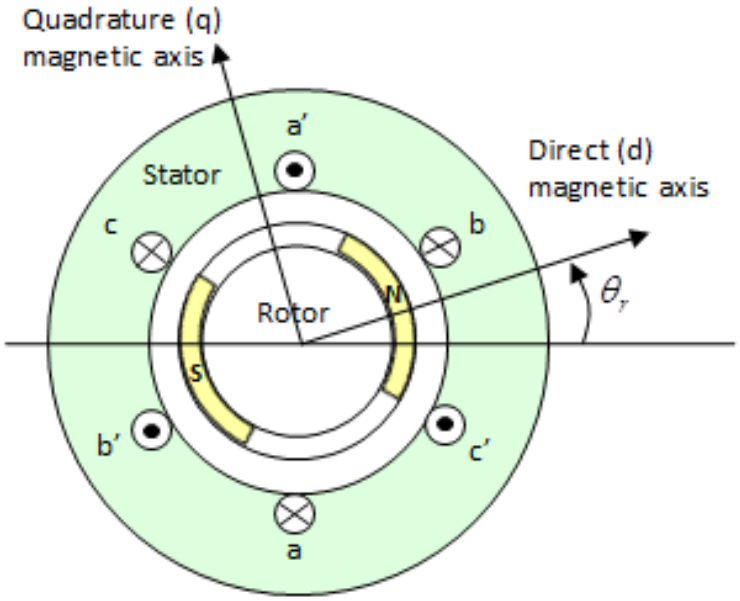

Figure 2.3: PM machine dq axis diagram [30].

From the alignment of d and q axis with the magnets, we have the flux linkage equations for d axis and q axis [29]

$$\lambda_d = L_d i_d + \lambda_{fd} \tag{2.22}$$

$$\lambda_q = L_q i_q \tag{2.23}$$

Modifying the equations, we have [29]

$$v_d = Ri_d + \frac{\partial(L_d i_d + \lambda_{fd})}{\partial t} - \omega_d L_q i_q \tag{2.24}$$

$$v_q = Ri_q + \frac{\partial L_q i_q}{\partial t} + \omega_d L_d i_d + \omega_d \lambda_{fd} \tag{2.25}$$

$$F_{pto} = \frac{\pi}{\tau}(L_d i_d i_q + \lambda_{fd} i_q - L_q i_d i_q) \tag{2.26}$$

2.3.2 DC generator modelling

In this section, a simple DC machine which has the voltage given by the equation [29]

$$v = iR + L\frac{\partial i}{\partial t} + k_e \omega = iR + L\frac{\partial i}{\partial t} + k_{lin}\dot{z} \tag{2.27}$$

where k_{lin} is the new back emf constant.

The equation for F_{pto} is proportional to current with the proportionality constant i.e. the torque constant being numerically equal to the back emf constant [29] :

$$F_{pto} = k_{lin} i \tag{2.28}$$

Notice that the dq model is non-linear and would require linearization before integrating it with the hydrodynamic model.

2.4 Taylor series expansions for non-linear state-space models

The formulation of MPC requires the plant model to be linear as MATLAB's quadratic programming works only for linear models. So, linearization of the dq model is required as per Taylor series expansions for non-linear state-space [31].

$$\dot{\mathbf{x}} = f(\mathbf{x}, \mathbf{u}) \qquad \mathbf{y} = g(\mathbf{x}, \mathbf{u}) \tag{2.29}$$

$$\mathbf{x} \in \Re^n \qquad \mathbf{u} \in \Re^m \qquad \mathbf{y} \in \Re^p \tag{2.30}$$

$$\underbrace{\dot{\mathbf{x}}_0 + \dot{\tilde{\mathbf{x}}}}_{\dot{\mathbf{x}}} = f(\mathbf{x}_0 + \tilde{\mathbf{x}}, \mathbf{u}_0 + \tilde{\mathbf{u}}) \approx \underbrace{f(\mathbf{x}_0, \mathbf{u}_0)}_{\dot{\mathbf{x}}_0} + \underbrace{\mathbf{A}\tilde{\mathbf{x}} + \mathbf{B}\tilde{\mathbf{u}}}_{\dot{\tilde{\mathbf{x}}}} \tag{2.31}$$

$$\underbrace{\mathbf{y}_0 + \tilde{\mathbf{y}}}_{\mathbf{y}} = g(\mathbf{x}_0 + \tilde{\mathbf{x}}, \mathbf{u}_0 + \tilde{\mathbf{u}}) \approx \underbrace{g(\mathbf{x}_0, \mathbf{u}_0)}_{\mathbf{y}_0} + \underbrace{\mathbf{C}\tilde{\mathbf{x}} + \mathbf{D}\tilde{\mathbf{u}}}_{\tilde{\mathbf{y}}} \tag{2.32}$$

$$\dot{\tilde{\mathbf{x}}} = \underbrace{\begin{bmatrix} \frac{\delta f_1}{\delta x_1} & \cdots & \frac{\delta f_1}{\delta x_n} \\ \vdots & \ddots & \vdots \\ \frac{\delta f_n}{\delta x_1} & \cdots & \frac{\delta f_n}{\delta x_n} \end{bmatrix}_{\mathbf{x}_0}}_{\mathbf{A}} \tilde{\mathbf{x}} + \underbrace{\begin{bmatrix} \frac{\delta f_1}{\delta u_1} & \cdots & \frac{\delta f_1}{\delta u_m} \\ \vdots & \ddots & \vdots \\ \frac{\delta f_n}{\delta u_1} & \cdots & \frac{\delta f_n}{\delta u_m} \end{bmatrix}_{\mathbf{u}_0}}_{\mathbf{B}} \tilde{\mathbf{u}} \tag{2.33}$$

$$\tilde{\mathbf{y}} = \underbrace{\begin{bmatrix} \frac{\delta g_1}{\delta x_1} & \cdots & \frac{\delta g_1}{\delta x_n} \\ \vdots & \ddots & \vdots \\ \frac{\delta g_p}{\delta x_1} & \cdots & \frac{\delta g_p}{\delta x_n} \end{bmatrix}_{\mathbf{x}_0}}_{\mathbf{C}} \tilde{\mathbf{x}} + \underbrace{\begin{bmatrix} \frac{\delta g_1}{\delta u_1} & \cdots & \frac{\delta f_1}{\delta u_m} \\ \vdots & \ddots & \vdots \\ \frac{\delta g_p}{\delta u_1} & \cdots & \frac{\delta g_p}{\delta u_m} \end{bmatrix}_{\mathbf{u}_0}}_{\mathbf{D}} \tilde{\mathbf{u}} \tag{2.34}$$

By substituting $\tilde{\mathbf{x}} = \mathbf{x} - \mathbf{x}_0$, $\tilde{\mathbf{u}} = \mathbf{u} - \mathbf{u}_0$, and $\tilde{\mathbf{y}} = \mathbf{y} - \mathbf{y}_0$:

$$\dot{\mathbf{x}} \approx \mathbf{A}\mathbf{x} + \mathbf{B}\mathbf{u} + f(\mathbf{x}_0, \mathbf{u}_0) - \mathbf{A}\mathbf{x_0} - \mathbf{B}\mathbf{u_0} \tag{2.35}$$

$$\mathbf{y} \approx \mathbf{C}\mathbf{x} + \mathbf{D}\mathbf{u} + g(\mathbf{x}_0, \mathbf{u}_0) - \mathbf{C}\mathbf{x_0} - \mathbf{D}\mathbf{u_0} \tag{2.36}$$

2.5 Linearization and integration of dq model with hydrodynamic model

State transition equations:

$$\frac{d}{dt}\begin{bmatrix} \dot{z} \\ z \\ F_r' \\ \int_{-\infty}^{t} F_r'\, d\tau \\ i_d \\ i_q \end{bmatrix} = f\left(\begin{bmatrix} \dot{z} \\ z \\ F_r' \\ \int_{-\infty}^{t} F_r'\, d\tau \\ i_d \\ i_q \end{bmatrix}, \begin{bmatrix} F_e \\ v_d \\ v_q \end{bmatrix}\right) \tag{2.37}$$

Output equations:

$$\begin{bmatrix} \dot{z} \\ z \\ F_{pto} \\ i_d \\ i_q \\ v_d \\ v_q \end{bmatrix} = g\left(\begin{bmatrix} \dot{z} \\ z \\ F_r' \\ \int_{-\infty}^{t} F_r'\, d\tau \\ i_d \\ i_q \end{bmatrix}, \begin{bmatrix} F_e \\ v_d \\ v_q \end{bmatrix}\right) \tag{2.38}$$

The hydrodynamic portion of the equation remains the same.

We also have

$$F_{pto} = \frac{\pi}{\tau}(L_d i_d i_q + \lambda_{fd} i_q - L_q i_d i_q) \tag{2.39}$$

The synchronous speed of the generator is directly proportional to the WEC speed

$$\omega_d = k_\omega \dot{z} \tag{2.40}$$

Say

$$mA = m + A(\infty) \tag{2.41}$$

$$\begin{aligned}
f_1 &= \frac{\partial}{\partial t}\dot{z} = \frac{-k}{mA}z + \frac{1}{mA}F_r' + \frac{1}{mA}\underbrace{\frac{\pi}{\tau}(L_d i_d i_q + \lambda_{fd} i_q - L_q i_d i_q)}_{F_{pto}} + \frac{1}{mA}F_e \\
f_2 &= \frac{\partial}{\partial t}z = \dot{z} \\
f_3 &= \frac{\partial}{\partial t}F_r' = -\frac{c_{aa}}{c_{ba}}\dot{z} - \frac{c_{ab}}{c_{ba}}z - \frac{c_{bb}}{c_{ba}}F_r' - \frac{c_{bc}}{c_{ba}}\int_{-\infty}^{t} F_r'\, d\tau \\
f_4 &= \frac{\partial}{\partial t}\int_{-\infty}^{t} F_r'\, d\tau = F_r' \\
f_5 &= \frac{\partial}{\partial t}i_d = \frac{-R}{L_d}i_d + \frac{k_\omega \dot{z} L_q}{L_d}i_q + \frac{1}{L_d}v_d \\
f_6 &= \frac{\partial}{\partial t}i_q = \frac{-k_\omega \dot{z} L_d}{L_q}i_d + \frac{-R}{L_q}i_q + \frac{1}{L_q}v_q - \frac{k_\omega \dot{z}\lambda_{fd}}{L_q}
\end{aligned} \tag{2.42}$$

Linearizing these w.r.t $\dot{z}, z, F_r', \int_{-\infty}^{t} F_r' i_d, i_q$ for A matrix and v_d, v_q, Fe for B matrix using Taylor series expansions as per equation 2.33 and putting them in state space format are discussed in the upcoming sections.

$$\mathbf{A} = \begin{bmatrix} 0 & \frac{-k}{mA} & \frac{1}{mA} & 0 & \frac{\pi}{\tau mA}(L_d - L_q)i_{q0} & \frac{\pi}{\tau mA}((L_d - L_q)i_{d0} + \lambda_{fd}) \\ 1 & 0 & 0 & 0 & 0 & 0 \\ -\frac{c_{aa}}{c_{ba}} & -\frac{c_{ab}}{c_{ba}} & -\frac{c_{bb}}{c_{ba}} & -\frac{c_{bc}}{c_{ba}} & 0 & 0 \\ 0 & 0 & 1 & 0 & 0 & 0 \\ \frac{k_\omega L_q i_{q0}}{L_d} & 0 & 0 & 0 & \frac{-R}{L_d} & \frac{k_\omega \dot{z_0} L_q}{L_d} \\ -(\frac{k_\omega L_d i_{d0}}{L_q} + \frac{k_\omega \lambda_{fd}}{L_q}) & 0 & 0 & 0 & \frac{-k_\omega \dot{z_0} L_d}{L_q} & \frac{-R}{L_q} \end{bmatrix} \tag{2.43}$$

$$\mathbf{B} = \begin{bmatrix} \frac{1}{mA} & 0 & 0 \\ 0 & 0 & 0 \\ 0 & 0 & 0 \\ 0 & 0 & 0 \\ 0 & \frac{1}{L_d} & 0 \\ 0 & 0 & \frac{1}{L_q} \end{bmatrix} \tag{2.44}$$

But

$$f(\mathbf{x}_0, \mathbf{u}_0) = \begin{bmatrix} \frac{-kz_0}{mA} + \frac{F'_{r0}}{mA} + \frac{\pi((L_d - L_q)i_{d0}i_{q0} + \lambda_{fd}i_{q0})}{\tau mA} + \frac{F_{e0}}{mA} \\ \dot{z_0} \\ -\frac{c_{aa}\dot{z_0}}{c_{ba}} - \frac{c_{ab}z_0}{c_{ba}} - \frac{c_{bb}F'_{ro}}{c_{ba}} - \frac{c_{bc}\left(\int_{-\infty}^{t} F'_r \, d\tau\right)_0}{c_{ba}} \\ F'_{ro} \\ \frac{-Ri_{d0}}{L_d} + \frac{k_\omega \dot{z_0} L_q i_{q0}}{L_d} + \frac{v_{d0}}{L_d} \\ -\frac{k_\omega \dot{z_0} L_d i_{d0}}{L_q} + \frac{-Ri_{q0}}{L_q} + \frac{v_{q0}}{L_q} - \frac{k_\omega \dot{z_0} \lambda_{fd}}{L_q} \end{bmatrix} \tag{2.45}$$

$$\mathbf{Ax}_0 = \begin{bmatrix} \frac{-kz_0}{mA} + \frac{F'_{r0}}{mA} + \frac{\pi(2(L_d - L_q)i_{d0}i_{q0} + \lambda_{fd}i_{q0})}{\tau mA} \\ \dot{z_0} \\ -\frac{c_{aa}\dot{z_0}}{c_{ba}} - \frac{c_{ab}z_0}{c_{ba}} - \frac{c_{bb}F'_{ro}}{c_{ba}} - \frac{c_{bc}\left(\int_{-\infty}^{t} F'_r \, d\tau\right)_0}{c_{ba}} \\ F'_{ro} \\ \frac{-Ri_{d0}}{L_d} + \frac{2k_\omega \dot{z_0} L_q i_{q0}}{L_d} \\ -\frac{2k_\omega \dot{z_0} L_d i_{d0}}{L_q} + \frac{-Ri_{q0}}{L_q} - \frac{k_\omega \dot{z_0} \lambda_{fd}}{L_q} \end{bmatrix} \tag{2.46}$$

$$\mathbf{Bu}_0 = \begin{bmatrix} \frac{F_{e0}}{mA} \\ 0 \\ 0 \\ 0 \\ \frac{v_{d0}}{L_d} \\ \frac{v_{q0}}{L_q} \end{bmatrix} \tag{2.47}$$

Substituting $f(\mathbf{x}_0, \mathbf{u}_0)$ in equation 2.35 and cancelling the repeated terms, we get our original $\mathbf{Ax}+\mathbf{Bu}$ since all the terms of $f(\mathbf{x}_0, \mathbf{u}_0)$ and $\mathbf{Ax}_o$,$\mathbf{Bu}_o$ get cancelled out. The calculations are shown below :

$$f(\mathbf{x}_0,\mathbf{u}_0)-(\mathbf{A}\mathbf{x}_o+\mathbf{B}\mathbf{u}_o)=$$

$$\begin{bmatrix} \frac{-kz_0}{mA}+\frac{F'_{r0}}{mA}+\frac{\pi((L_d-L_q)i_{d0}i_{q0}+\lambda_{fd}i_{q0})}{\tau mA}+\frac{F_{e0}}{mA} \\ \dot{z_0} \\ -\frac{c_{aa}\dot{z_0}}{c_{ba}}-\frac{c_{ab}z_0}{c_{ba}}-\frac{c_{bb}F'_{ro}}{c_{ba}}-\frac{c_{bc}\left(\int_{-\infty}^{t}F'_r\,d\tau\right)_0}{c_{ba}} \\ F'_{ro} \\ \frac{-Ri_{d0}}{L_d}+\frac{k_\omega z_0 L_q i_{q0}}{L_d}+\frac{v_{d0}}{L_d} \\ -\frac{k_\omega z_0 L_d i_{d0}}{L_q}+\frac{-Ri_{q0}}{L_q}+\frac{v_{q0}}{L_q}-\frac{k_\omega z_0\lambda_{fd}}{L_q} \end{bmatrix} - \begin{bmatrix} \frac{-kz_0}{mA}+\frac{F'_{r0}}{mA}+\frac{\pi(2(L_d-L_q)i_{d0}i_{q0}+\lambda_{fd}i_{q0})}{\tau mA} \\ \dot{z_0} \\ -\frac{c_{aa}\dot{z_0}}{c_{ba}}-\frac{c_{ab}z_0}{c_{ba}}-\frac{c_{bb}F'_{ro}}{c_{ba}}-\frac{c_{bc}\left(\int_{-\infty}^{t}F'_r\,d\tau\right)_0}{c_{ba}} \\ F'_{ro} \\ \frac{-Ri_{d0}}{L_d}+\frac{2k_\omega z_0 L_q i_{q0}}{L_d} \\ -\frac{2k_\omega z_0 L_d i_{d0}}{L_q}+\frac{-Ri_{q0}}{L_q}-\frac{k_\omega z_0\lambda_{fd}}{L_q} \end{bmatrix} - \begin{bmatrix} \frac{F_{e0}}{mA} \\ 0 \\ 0 \\ 0 \\ \frac{v_{d0}}{L_d} \\ \frac{v_{q0}}{L_q} \end{bmatrix} \tag{2.48}$$

$$f(\mathbf{x}_0,\mathbf{u}_0)-(\mathbf{A}\mathbf{x}_o+\mathbf{B}\mathbf{u}_o)=\begin{bmatrix} -\frac{\pi(L_d-L_q)i_{d0}i_{q0}}{\tau mA} \\ 0 \\ 0 \\ 0 \\ -\frac{k_\omega z_0 L_q i_{q0}}{L_d} \\ +\frac{k_\omega z_0 L_d i_{d0}}{L_q} \end{bmatrix} \tag{2.49}$$

Substituting the values back into equation 2.35

$$\frac{d}{dt}\begin{bmatrix} \dot{z} \\ z \\ F_r' \\ \int_{-\infty}^{t} F_r'\, d\tau \\ i_d \\ i_q \end{bmatrix}$$

$$= \begin{bmatrix} 0 & \frac{-k}{mA} & \frac{1}{mA} & 0 & \frac{\pi}{\tau mA}(L_d - L_q) i_{q0} & \frac{\pi}{\tau mA}((L_d - L_q) i_{d0} + \lambda_{fd}) \\ 1 & 0 & 0 & 0 & 0 & 0 \\ -\frac{c_{aa}}{c_{ba}} & -\frac{c_{ab}}{c_{ba}} & -\frac{c_{bb}}{c_{ba}} & -\frac{c_{bc}}{c_{ba}} & 0 & 0 \\ 0 & 0 & 1 & 0 & 0 & 0 \\ \frac{k_\omega L_q i_{q0}}{L_d} & 0 & 0 & 0 & \frac{-R}{L_d} & \frac{k_\omega \dot{z_0} L_q}{L_d} \\ -(\frac{k_\omega L_d i_{d0}}{L_q} + \frac{k_\omega \lambda_{fd}}{L_q}) & 0 & 0 & 0 & \frac{-k_\omega \dot{z_0} L_d}{L_q} & \frac{-R}{L_q} \end{bmatrix}$$

$$\begin{bmatrix} \dot{z} \\ z \\ F_r' \\ \int_{-\infty}^{t} F_r'\, d\tau \\ i_d \\ i_q \end{bmatrix} + \begin{bmatrix} \frac{1}{mA} & 0 & 0 \\ 0 & 0 & 0 \\ 0 & 0 & 0 \\ 0 & 0 & 0 \\ 0 & \frac{1}{L_d} & 0 \\ 0 & 0 & \frac{1}{L_q} \end{bmatrix} \begin{bmatrix} F_e \\ v_d \\ v_q \end{bmatrix} + \begin{bmatrix} -\frac{\pi(L_d - L_q) i_{d0} i_{q0}}{\tau mA} \\ 0 \\ 0 \\ -\frac{k_\omega \dot{z_0} L_q i_{q0}}{L_d} \\ +\frac{k_\omega \dot{z_0} L_d i_{d0}}{L_q} \end{bmatrix} \quad (2.50)$$

So, the input set of equations after simplification and rearrangement will be :

$$\frac{d}{dt}\begin{bmatrix} \dot{z} \\ z \\ F_r' \\ \int_{-\infty}^{t} F_r'\, d\tau \\ i_d \\ i_q \end{bmatrix} = \underbrace{\begin{bmatrix} 0 & \frac{-k}{mA} & \frac{1}{mA} & 0 & \frac{\pi}{\tau mA}(L_d - L_q) i_{q0} & \frac{\pi}{\tau mA}((L_d - L_q) i_{d0} + \lambda_{fd}) \\ 1 & 0 & 0 & 0 & 0 & 0 \\ -\frac{c_{aa}}{c_{ba}} & -\frac{c_{ab}}{c_{ba}} & -\frac{c_{bb}}{c_{ba}} & -\frac{c_{bc}}{c_{ba}} & 0 & 0 \\ 0 & 0 & 1 & 0 & 0 & 0 \\ \frac{k_\omega L_q i_{q0}}{L_d} & 0 & 0 & 0 & \frac{-R}{L_d} & \frac{k_\omega \dot{z_0} L_q}{L_d} \\ -(\frac{k_\omega L_d i_{d0}}{L_q} + \frac{k_\omega \lambda_{fd}}{L_q}) & 0 & 0 & 0 & \frac{-k_\omega \dot{z_0} L_d}{L_q} & \frac{-R}{L_q} \end{bmatrix}}_{\mathbf{A}} \begin{bmatrix} \dot{z} \\ z \\ F_r' \\ \int_{-\infty}^{t} F_r'\, d\tau \\ i_d \\ i_q \end{bmatrix} + \underbrace{\begin{bmatrix} 0 & 0 \\ 0 & 0 \\ 0 & 0 \\ 0 & 0 \\ \frac{1}{L_d} & 0 \\ 0 & \frac{1}{L_q} \end{bmatrix}}_{\mathbf{B}_u} \begin{bmatrix} v_d \\ v_q \end{bmatrix} + \underbrace{\begin{bmatrix} \frac{1}{mA} & -\frac{\pi(L_d - L_q) i_{d0} i_{q0}}{\tau mA} \\ 0 & 0 \\ 0 & 0 \\ 0 & 0 \\ 0 & -\frac{k_\omega \dot{z_0} L_q i_{q0}}{L_d} \\ 0 & +\frac{k_\omega \dot{z_0} L_d i_{d0}}{L_q} \end{bmatrix}}_{\mathbf{B}_v} \begin{bmatrix} F_e \\ 1 \end{bmatrix} \quad (2.51)$$

Repeating the same process for the output equations, we get

$$\begin{aligned}
\dot{z} &= g_1 = \dot{z} \\
z &= g_2 = z \\
F_{pto} &= g_3 = \frac{\pi}{\tau}(L_d i_d i_q + \lambda_{fd} i_q - L_q i_d i_q) \\
i_d &= g_4 = i_d \\
i_q &= g_5 = i_q \\
v_d &= g_6 = v_d \\
v_q &= g_7 = v_q
\end{aligned} \tag{2.52}$$

$$\mathbf{C} = \begin{bmatrix} 1 & 0 & 0 & 0 & 0 & 0 \\ 0 & 1 & 0 & 0 & 0 & 0 \\ 0 & 0 & 0 & 0 & \frac{\pi}{\tau}(L_d - L_q)i_{q0} & \frac{\pi}{\tau}(L_d - L_q)i_{d0} + \frac{\pi}{\tau}\lambda_{fd} \\ 0 & 0 & 0 & 0 & 1 & 0 \\ 0 & 0 & 0 & 0 & 0 & 1 \\ 0 & 0 & 0 & 0 & 0 & 0 \\ 0 & 0 & 0 & 0 & 0 & 0 \end{bmatrix} \tag{2.53}$$

$$\mathbf{D} = \begin{bmatrix} 0 & 0 & 0 \\ 0 & 0 & 0 \\ 0 & 0 & 0 \\ 0 & 0 & 0 \\ 0 & 0 & 0 \\ 0 & 1 & 0 \\ 0 & 0 & 1 \end{bmatrix} \tag{2.54}$$

$$g(\mathbf{x}_0, \mathbf{u}_0) = \begin{bmatrix} \dot{z}_o \\ z_o \\ \frac{\pi}{\tau}(L_d - L_q)i_{d0}i_{q0} + \frac{\pi}{\tau}\lambda_{fd}i_{q0} \\ i_{d0} \\ i_{q0} \\ v_{d0} \\ v_{q0} \end{bmatrix} \tag{2.55}$$

$$\mathbf{Cx}_0 = \begin{bmatrix} \dot{z}_o \\ z_o \\ \frac{\pi}{\tau}(L_d - L_q) i_{d0} i_{q0} + \frac{\pi}{\tau}(L_d - L_q) i_{d0} i_{q0} + \frac{\pi}{\tau}\lambda_{fd} i_{q0} \\ i_{d0} \\ i_{q0} \\ 0 \\ 0 \end{bmatrix} \tag{2.56}$$

$$\mathbf{Du}_0 = \begin{bmatrix} 0 \\ 0 \\ 0 \\ 0 \\ 0 \\ v_{d0} \\ v_{q0} \end{bmatrix} \tag{2.57}$$

Simplifying this using taylor series expansions for non-linear state-space as per equation 2.36, $g(\mathbf{x}_0, \mathbf{u}_0)$ cancels out $\mathbf{Cx}_0$ and $\mathbf{Du}_0$ The calculations are shown below :

$$g(\mathbf{x}_0, \mathbf{u}_0) - (\mathbf{C}\mathbf{x}_o + \mathbf{D}\mathbf{u}_o) =$$

$$\begin{bmatrix} \dot{z}_o \\ z_o \\ \frac{\pi}{\tau}(L_d - L_q) i_{d0} i_{q0} + \frac{\pi}{\tau}\lambda_{fd} i_{q0} \\ i_{d0} \\ i_{q0} \\ v_{d0} \\ v_{q0} \end{bmatrix} - \begin{bmatrix} \dot{z}_o \\ z_o \\ \frac{\pi}{\tau}(L_d - L_q) i_{d0} i_{q0} + \frac{\pi}{\tau}(L_d - L_q) i_{d0} i_{q0} + \frac{\pi}{\tau}\lambda_{fd} i_{q0} \\ i_{d0} \\ i_{q0} \\ 0 \\ 0 \end{bmatrix} - \begin{bmatrix} 0 \\ 0 \\ 0 \\ 0 \\ 0 \\ v_{d0} \\ v_{q0} \end{bmatrix} \tag{2.58}$$

$$g(\mathbf{x}_0, \mathbf{u}_0) - (\mathbf{C}\mathbf{x}_o + \mathbf{D}\mathbf{u}_o) = \begin{bmatrix} 0 \\ 0 \\ -\frac{\pi}{\tau}(L_d - L_q) i_{d0} i_{q0} \\ 0 \\ 0 \\ 0 \\ 0 \end{bmatrix} \tag{2.59}$$

Substituting the values back into equation 2.36

$$\begin{bmatrix} \dot{z} \\ z \\ F_{pto} \\ i_d \\ i_q \\ v_d \\ v_q \end{bmatrix} = \begin{bmatrix} 1 & 0 & 0 & 0 & 0 & 0 \\ 0 & 1 & 0 & 0 & 0 & 0 \\ 0 & 0 & 0 & 0 & \frac{\pi}{\tau}(L_d - L_q)i_{q0} & \frac{\pi}{\tau}(L_d - L_q)i_{d0} + \frac{\pi}{\tau}\lambda_{fd} \\ 0 & 0 & 0 & 0 & 1 & 0 \\ 0 & 0 & 0 & 0 & 0 & 1 \\ 0 & 0 & 0 & 0 & 0 & 0 \\ 0 & 0 & 0 & 0 & 0 & 0 \end{bmatrix} \begin{bmatrix} \dot{z} \\ z \\ F'_r \\ \int_{-\infty}^{t} F'_r \, d\tau \\ i_d \\ i_q \end{bmatrix} + \begin{bmatrix} 0 & 0 & 0 \\ 0 & 0 & 0 \\ 0 & 0 & 0 \\ 0 & 0 & 0 \\ 0 & 0 & 0 \\ 0 & 1 & 0 \\ 0 & 0 & 1 \end{bmatrix} \begin{bmatrix} Fe \\ v_d \\ v_q \end{bmatrix}$$

$$\begin{bmatrix} 0 \\ 0 \\ -\frac{\pi}{\tau}(L_d - L_q)i_{d0}i_{q0} \\ 0 \\ 0 \\ 0 \\ 0 \end{bmatrix} + \quad (2.60)$$

After simplification and rearrangement, the output equations are :

$$\begin{bmatrix} \dot{z} \\ z \\ F_{pto} \\ i_d \\ i_q \\ v_d \\ v_q \end{bmatrix} = \underbrace{\begin{bmatrix} 1 & 0 & 0 & 0 & 0 & 0 \\ 0 & 1 & 0 & 0 & 0 & 0 \\ 0 & 0 & 0 & 0 & \frac{\pi}{\tau}(L_d - L_q)i_{q0} & \frac{\pi}{\tau}(L_d - L_q)i_{d0} + \frac{\pi}{\tau}\lambda_{fd} \\ 0 & 0 & 0 & 0 & 1 & 0 \\ 0 & 0 & 0 & 0 & 0 & 1 \\ 0 & 0 & 0 & 0 & 0 & 0 \\ 0 & 0 & 0 & 0 & 0 & 0 \end{bmatrix}}_{\mathbf{C}} \begin{bmatrix} \dot{z} \\ z \\ F_r' \\ \int_{-\infty}^{t} F_r' \, d\tau \\ i_d \\ i_q \end{bmatrix} + \underbrace{\begin{bmatrix} 0 & 0 \\ 0 & 0 \\ 0 & 0 \\ 0 & 0 \\ 0 & 0 \\ 1 & 0 \\ 0 & 1 \end{bmatrix}}_{\mathbf{D}_u} \begin{bmatrix} v_d \\ v_q \end{bmatrix} + \underbrace{\begin{bmatrix} 0 & 0 \\ 0 & 0 \\ 0 & -\frac{\pi}{\tau}(L_d - L_q)i_{d0}i_{q0} \\ 0 & 0 \\ 0 & 0 \\ 0 & 0 \\ 0 & 0 \end{bmatrix}}_{\mathbf{D}_v} \begin{bmatrix} F_e \\ 1 \end{bmatrix} \tag{2.61}$$

Final input and output equations are :

$$\frac{d}{dt}\begin{bmatrix} \dot{z} \\ z \\ F_r' \\ \int_{-\infty}^{t} F_r'\, d\tau \\ i_d \\ i_q \end{bmatrix}$$

$$= \underbrace{\begin{bmatrix} 0 & \frac{-k}{mA} & \frac{1}{mA} & 0 & \frac{\pi}{\tau(mA)}(L_d - L_q) i_{q0} & \frac{\pi}{\tau(mA)}((L_d - L_q) i_{d0} + \lambda_{fd}) \\ 1 & 0 & 0 & 0 & 0 & 0 \\ -\frac{c_{aa}}{c_{ba}} & -\frac{c_{ab}}{c_{ba}} & -\frac{c_{bb}}{c_{ba}} & -\frac{c_{bc}}{c_{ba}} & 0 & 0 \\ 0 & 0 & 1 & 0 & 0 & 0 \\ \frac{k_\omega L_q i_{q0}}{L_d} & 0 & 0 & 0 & \frac{-R}{L_d} & \frac{k_\omega \dot{z_0} L_q}{L_d} \\ -(\frac{k_\omega L_d i_{d0}}{L_q} + \frac{k_\omega \lambda_{fd}}{L_q}) & 0 & 0 & 0 & \frac{-k_\omega \dot{z_0} L_d}{L_q} & \frac{-R}{L_q} \end{bmatrix}}_{\mathbf{A}}$$

$$\begin{bmatrix} \dot{z} \\ z \\ F_r' \\ \int_{-\infty}^{t} F_r'\, d\tau \\ i_d \\ i_q \end{bmatrix}$$

$$+ \underbrace{\begin{bmatrix} 0 & 0 \\ 0 & 0 \\ 0 & 0 \\ 0 & 0 \\ \frac{1}{L_d} & 0 \\ 0 & \frac{1}{L_q} \end{bmatrix}}_{\mathbf{B}_u} \begin{bmatrix} v_d \\ v_q \end{bmatrix} + \underbrace{\begin{bmatrix} \frac{1}{mA} & -\frac{\pi(L_d - L_q) i_{d0} i_{q0}}{\tau mA} \\ 0 & 0 \\ 0 & 0 \\ 0 & 0 \\ 0 & -\frac{k_\omega \dot{z_0} L_q i_{q0}}{L_d} \\ 0 & +\frac{k_\omega \dot{z_0} L_d i_{d0}}{L_q} \end{bmatrix}}_{\mathbf{B}_v} \begin{bmatrix} F_e \\ 1 \end{bmatrix} \quad (2.62)$$

$$\begin{bmatrix} \dot{z} \\ z \\ F_{pto} \\ i_d \\ i_q \\ v_d \\ v_q \end{bmatrix} = \underbrace{\begin{bmatrix} 1 & 0 & 0 & 0 & 0 & 0 \\ 0 & 1 & 0 & 0 & 0 & 0 \\ 0 & 0 & 0 & 0 & \frac{\pi}{\tau}(L_d - L_q)i_{q0} & \frac{\pi}{\tau}(L_d - L_q)i_{d0} + \frac{\pi}{\tau}\lambda_{fd} \\ 0 & 0 & 0 & 0 & 1 & 0 \\ 0 & 0 & 0 & 0 & 0 & 1 \\ 0 & 0 & 0 & 0 & 0 & 0 \\ 0 & 0 & 0 & 0 & 0 & 0 \end{bmatrix}}_{\mathbf{C}} \begin{bmatrix} \dot{z} \\ z \\ F_r' \\ \int_{-\infty}^{t} F_r' \, d\tau \\ i_d \\ i_q \end{bmatrix} + \underbrace{\begin{bmatrix} 0 & 0 \\ 0 & 0 \\ 0 & 0 \\ 0 & 0 \\ 0 & 0 \\ 1 & 0 \\ 0 & 1 \end{bmatrix}}_{\mathbf{D}_u} \begin{bmatrix} v_d \\ v_q \end{bmatrix} + \underbrace{\begin{bmatrix} 0 & 0 \\ 0 & 0 \\ 0 & -\frac{\pi}{\tau}(L_d - L_q)i_{d0}i_{q0} \\ 0 & 0 \\ 0 & 0 \\ 0 & 0 \\ 0 & 0 \end{bmatrix}}_{\mathbf{D}_v} \begin{bmatrix} F_e \\ 1 \end{bmatrix} \tag{2.63}$$

2.5.1 Re-arrangement of linearization points

By rearranging the disturbances entirely, the equations can be written as follows. But this might require updating the A matrix constantly since $i_{d0}, i_{q0}, \dot{z_0}$ are being predicted for every time step.

$$\frac{d}{dt}\begin{bmatrix} \dot{z} \\ z \\ F_r' \\ \int_{-\infty}^{t} F_r'\, d\tau \\ i_d \\ i_q \end{bmatrix} = \underbrace{\begin{bmatrix} 0 & \frac{-k}{mA} & \frac{1}{mA} & 0 & \frac{\pi}{\tau(mA)}(L_d - L_q)i_{q0} & \frac{\pi}{\tau(mA)}((L_d - L_q)i_{d0} + \lambda_{fd}) \\ 1 & 0 & 0 & 0 & 0 & 0 \\ -\frac{c_{aa}}{c_{ba}} & -\frac{c_{ab}}{c_{ba}} & -\frac{c_{bb}}{c_{ba}} & -\frac{c_{bc}}{c_{ba}} & 0 & 0 \\ 0 & 0 & 1 & 0 & 0 & 0 \\ \frac{k_\omega L_q i_{q0}}{L_d} & 0 & 0 & 0 & \frac{-R}{L_d} & \frac{k_\omega \dot{z_0} L_q}{L_d} \\ -(\frac{k_\omega L_d i_{d0}}{L_q} + \frac{k_\omega \lambda_{fd}}{L_q}) & 0 & 0 & 0 & \frac{-k_\omega \dot{z_0} L_d}{L_q} & \frac{-R}{L_q} \end{bmatrix}}_{\mathbf{A}} \begin{bmatrix} \dot{z} \\ z \\ F_r' \\ \int_{-\infty}^{t} F_r'\, d\tau \\ i_d \\ i_q \end{bmatrix} + \underbrace{\begin{bmatrix} 0 & 0 \\ 0 & 0 \\ 0 & 0 \\ 0 & 0 \\ \frac{1}{L_d} & 0 \\ 0 & \frac{1}{L_q} \end{bmatrix}}_{\mathbf{B}_u} \begin{bmatrix} v_d \\ v_q \end{bmatrix} + \underbrace{\begin{bmatrix} \frac{1}{mA} & -\frac{\pi(L_d - L_q)}{\tau mA} & 0 & 0 \\ 0 & 0 & 0 & 0 \\ 0 & 0 & 0 & 0 \\ 0 & 0 & 0 & 0 \\ 0 & 0 & 0 & -\frac{k_\omega L_q}{L_d} \\ 0 & 0 & +\frac{k_\omega L_d}{L_q} & 0 \end{bmatrix}}_{\mathbf{B}_v} \begin{bmatrix} F_e \\ i_{d0} i_{q0} \\ i_{d0} \dot{z_0} \\ i_{q0} \dot{z_0} \end{bmatrix} \tag{2.64}$$

$$\begin{bmatrix} \dot{z} \\ z \\ F_{pto} \\ i_d \\ i_q \\ v_d \\ v_q \end{bmatrix} = \underbrace{\begin{bmatrix} 1 & 0 & 0 & 0 & 0 & 0 \\ 0 & 1 & 0 & 0 & 0 & 0 \\ 0 & 0 & 0 & 0 & \frac{\pi}{\tau}(L_d - L_q)i_{q0} & \frac{\pi}{\tau}(L_d - L_q)i_{d0} + \frac{\pi}{\tau}\lambda_{fd} \\ 0 & 0 & 0 & 0 & 1 & 0 \\ 0 & 0 & 0 & 0 & 0 & 1 \\ 0 & 0 & 0 & 0 & 0 & 0 \\ 0 & 0 & 0 & 0 & 0 & 0 \end{bmatrix}}_{\mathbf{C}} \begin{bmatrix} \dot{z} \\ z \\ F_r' \\ \int_{-\infty}^{t} F_r' \, d\tau \\ i_d \\ i_q \end{bmatrix} + \underbrace{\begin{bmatrix} 0 & 0 \\ 0 & 0 \\ 0 & 0 \\ 0 & 0 \\ 0 & 0 \\ 1 & 0 \\ 0 & 1 \end{bmatrix}}_{\mathbf{D}_u} \begin{bmatrix} v_d \\ v_q \end{bmatrix} + \underbrace{\begin{bmatrix} 0 & 0 & 0 & 0 \\ 0 & 0 & 0 & 0 \\ 0 & -\frac{\pi}{\tau}(L_d - L_q) & 0 & 0 \\ 0 & 0 & 0 & 0 \\ 0 & 0 & 0 & 0 \\ 0 & 0 & 0 & 0 \\ 0 & 0 & 0 & 0 \end{bmatrix}}_{\mathbf{D}_v} \begin{bmatrix} F_e \\ i_{d0}i_{q0} \\ i_{d0}\dot{z}_0 \\ i_{q0}\dot{z}_0 \end{bmatrix} \tag{2.65}$$

In equation 2.7, if friction force is also considered then the losses due to friction needs to be evaluated as well which is around ten percent of the rated power.

$$\frac{d}{dt}\begin{bmatrix} \dot{z} \\ z \\ F_r' \\ \int_{-\infty}^{t} F_r'\, d\tau \\ i_d \\ i_q \end{bmatrix} = \underbrace{\begin{bmatrix} \frac{-k_{fric}}{mA} & \frac{-k}{mA} & \frac{1}{mA} & 0 & \frac{\pi}{\tau(mA)}(L_d - L_q)i_{q0} & \frac{\pi}{\tau(mA)}((L_d - L_q)i_{d0} + \lambda_{fd}) \\ 1 & 0 & 0 & 0 & 0 & 0 \\ -\frac{c_{aa}}{c_{ba}} & -\frac{c_{ab}}{c_{ba}} & -\frac{c_{bb}}{c_{ba}} & -\frac{c_{bc}}{c_{ba}} & 0 & 0 \\ 0 & 0 & 1 & 0 & 0 & 0 \\ \frac{k_\omega L_q i_{q0}}{L_d} & 0 & 0 & 0 & \frac{-R}{L_d} & \frac{k_\omega \dot{z_0} L_q}{L_d} \\ -(\frac{k_\omega L_d i_{d0}}{L_q} + \frac{k_\omega \lambda_{fd}}{L_q}) & 0 & 0 & 0 & \frac{-k_\omega \dot{z_0} L_d}{L_q} & \frac{-R}{L_q} \end{bmatrix}}_{\mathbf{A}} \begin{bmatrix} \dot{z} \\ z \\ F_r' \\ \int_{-\infty}^{t} F_r'\, d\tau \\ i_d \\ i_q \end{bmatrix} + \underbrace{\begin{bmatrix} 0 & 0 \\ 0 & 0 \\ 0 & 0 \\ 0 & 0 \\ \frac{1}{L_d} & 0 \\ 0 & \frac{1}{L_q} \end{bmatrix}}_{\mathbf{B}_u} \begin{bmatrix} v_d \\ v_q \end{bmatrix} + \underbrace{\begin{bmatrix} \frac{1}{mA} & -\frac{\pi(L_d - L_q)}{\tau mA} & 0 & 0 \\ 0 & 0 & 0 & 0 \\ 0 & 0 & 0 & 0 \\ 0 & 0 & 0 & 0 \\ 0 & 0 & 0 & -\frac{k_\omega L_q}{L_d} \\ 0 & 0 & +\frac{k_\omega L_d}{L_q} & 0 \end{bmatrix}}_{\mathbf{B}_v} \begin{bmatrix} F_e \\ i_{d0} i_{q0} \\ i_{d0} \dot{z_0} \\ i_{q0} \dot{z_0} \end{bmatrix} \tag{2.66}$$

$$\begin{bmatrix} \dot{z} \\ z \\ F_{pto} \\ i_d \\ i_q \\ v_d \\ v_q \end{bmatrix} = \underbrace{\begin{bmatrix} 1 & 0 & 0 & 0 & 0 & 0 \\ 0 & 1 & 0 & 0 & 0 & 0 \\ 0 & 0 & 0 & 0 & \frac{\pi}{\tau}(L_d - L_q)i_{q0} & \frac{\pi}{\tau}(L_d - L_q)i_{d0} + \frac{\pi}{\tau}\lambda_{fd} \\ 0 & 0 & 0 & 0 & 1 & 0 \\ 0 & 0 & 0 & 0 & 0 & 1 \\ 0 & 0 & 0 & 0 & 0 & 0 \\ 0 & 0 & 0 & 0 & 0 & 0 \end{bmatrix}}_{\mathbf{C}} \begin{bmatrix} \dot{z} \\ z \\ F_r' \\ \int_{-\infty}^{t} F_r' \, d\tau \\ i_d \\ i_q \end{bmatrix} + \underbrace{\begin{bmatrix} 0 & 0 \\ 0 & 0 \\ 0 & 0 \\ 0 & 0 \\ 0 & 0 \\ 1 & 0 \\ 0 & 1 \end{bmatrix}}_{\mathbf{D}_u} \begin{bmatrix} v_d \\ v_q \end{bmatrix} + \underbrace{\begin{bmatrix} 0 & 0 & 0 & 0 \\ 0 & 0 & 0 & 0 \\ 0 & -\frac{\pi}{\tau}(L_d - L_q) & 0 & 0 \\ 0 & 0 & 0 & 0 \\ 0 & 0 & 0 & 0 \\ 0 & 0 & 0 & 0 \\ 0 & 0 & 0 & 0 \end{bmatrix}}_{\mathbf{D}_v} \begin{bmatrix} F_e \\ i_{d0}i_{q0} \\ i_{d0}\dot{z}_0 \\ i_{q0}\dot{z}_0 \end{bmatrix} \tag{2.67}$$

2.5.2 Formulation w.r.t. rate of change of current as control inputs

The above model can be modified to have rate of change of currents in d,q as the control inputs.

$$\frac{d}{dt}\begin{bmatrix} \dot{z} \\ z \\ F_r' \\ \int_{-\infty}^{t} F_r'\, d\tau \\ i_d \\ i_q \end{bmatrix}$$

$$= \underbrace{\begin{bmatrix} 0 & \frac{-k}{mA} & \frac{1}{mA} & 0 & \frac{\pi}{\tau(mA)}(L_d - L_q) i_{q0} & \frac{\pi}{\tau(mA)}((L_d - L_q) i_{d0} + \lambda_{fd}) \\ 1 & 0 & 0 & 0 & 0 & 0 \\ -\frac{c_{aa}}{c_{ba}} & -\frac{c_{ab}}{c_{ba}} & -\frac{c_{bb}}{c_{ba}} & -\frac{c_{bc}}{c_{ba}} & 0 & 0 \\ 0 & 0 & 1 & 0 & 0 & 0 \\ 0 & 0 & 0 & 0 & 0 & 0 \\ 0 & 0 & 0 & 0 & 0 & 0 \end{bmatrix}}_{\mathbf{A}}$$

$$\begin{bmatrix} \dot{z} \\ z \\ F_r' \\ \int_{-\infty}^{t} F_r'\, d\tau \\ i_d \\ i_q \end{bmatrix}$$

$$+ \underbrace{\begin{bmatrix} 0 & 0 \\ 0 & 0 \\ 0 & 0 \\ 0 & 0 \\ 1 & 0 \\ 0 & 1 \end{bmatrix}}_{\mathbf{B}_u} \begin{bmatrix} \frac{did}{dt} \\ \frac{diq}{dt} \end{bmatrix} + \underbrace{\begin{bmatrix} \frac{1}{mA} & -\frac{\pi(L_d - L_q) i_{d0} i_{q0}}{\tau mA} \\ 0 & 0 \\ 0 & 0 \\ 0 & 0 \\ 0 & 0 \\ 0 & 0 \end{bmatrix}}_{\mathbf{B}_v} \begin{bmatrix} F_e \\ 1 \end{bmatrix} \tag{2.68}$$

$$
\begin{bmatrix} \dot{z} \\ z \\ F_{pto} \\ i_d \\ i_q \\ v_d \\ v_q \end{bmatrix} = \underbrace{\begin{bmatrix} 1 & 0 & 0 & 0 & 0 & 0 \\ 0 & 1 & 0 & 0 & 0 & 0 \\ 0 & 0 & 0 & 0 & \frac{\pi}{\tau}(L_d - L_q) i_{q0} & \frac{\pi}{\tau}(L_d - L_q) i_{d0} + \frac{\pi}{\tau}\lambda_{fd} \\ 0 & 0 & 0 & 0 & 1 & 0 \\ 0 & 0 & 0 & 0 & 0 & 1 \\ -k_\omega L_q i_{qo} & 0 & 0 & 0 & R & -k_\omega \dot{z_0} L_q \\ (k_\omega L_d i_{do} + k_\omega \lambda_{fd}) & 0 & 0 & 0 & k_\omega \dot{z_0} L_d & R \end{bmatrix}}_{\mathbf{C}} \begin{bmatrix} \dot{z} \\ z \\ F_r' \\ \int_{-\infty}^{t} F_r' \, d\tau \\ i_d \\ i_q \end{bmatrix}
$$

$$
+ \underbrace{\begin{bmatrix} 0 & 0 \\ 0 & 0 \\ 0 & 0 \\ 0 & 0 \\ 0 & 0 \\ \frac{1}{L_d} & 0 \\ 0 & \frac{1}{L_q} \end{bmatrix}}_{\mathbf{D}_u} \begin{bmatrix} \frac{did}{dt} \\ \frac{diq}{dt} \end{bmatrix} +
$$

$$
\underbrace{\begin{bmatrix} 0 & 0 \\ 0 & 0 \\ 0 & -\frac{\pi}{\tau}(L_d - L_q) i_{d0} i_{q0} \\ 0 & 0 \\ 0 & 0 \\ 0 & k_\omega \dot{z_0} L_q i_{q0} \\ 0 & -k_\omega \dot{z_0} L_d i_{d0} \end{bmatrix}}_{\mathbf{D}_v} \begin{bmatrix} F_e \\ 1 \end{bmatrix}
$$

(2.69)

2.6 Integration of hydrodynamic model for a DC machine

Rewriting the equations discussed in 2.3.2,

$$v = iR + L\frac{\partial i}{\partial t} + k_e\omega = iR + L\frac{\partial i}{\partial t} + k_{lin}\dot{z} \tag{2.70}$$

where K_{lin} is the new back emf constant.

The equation for F_{pto} is proportional to current with the proportionality constant i.e. the torque constant being numerically equal to the back emf constant :

$$F_{pto} = k_{lin}i \tag{2.71}$$

Since the equations are linear, the input set of equations are given by :

$$\begin{aligned}
f_1 &= \frac{\partial}{\partial t}\dot{z} = \frac{-k}{mA}z + \frac{1}{mA}F_r' + \frac{1}{mA}\underbrace{k_{lin}i}_{F_{pto}} + \frac{1}{mA}F_e \\
f_2 &= \frac{\partial}{\partial t}z = \dot{z} \\
f_3 &= \frac{\partial}{\partial t}F_r' = -\frac{c_{aa}}{c_{ba}}\dot{z} - \frac{c_{ab}}{c_{ba}}z - \frac{c_{bb}}{c_{ba}}F_r' - \frac{c_{bc}}{c_{ba}}\int_{-\infty}^{t} F_r'\, d\tau \\
f_4 &= \frac{\partial}{\partial t}\int_{-\infty}^{t} F_r'\, d\tau = F_r' \\
f_5 &= \frac{\partial}{\partial t}i = \frac{-R}{L}i - \frac{k_{lin}\dot{z}}{L} + \frac{1}{L}v
\end{aligned} \tag{2.72}$$

Arranging them in state-space, we get :

$$\frac{d}{dt}\begin{bmatrix} \dot{z} \\ z \\ F_r' \\ \int_{-\infty}^{t} F_r' \, d\tau \\ i \end{bmatrix} = \underbrace{\begin{bmatrix} 0 & \frac{-k}{mA} & \frac{1}{mA} & 0 & \frac{k_{lin}}{mA} \\ 1 & 0 & 0 & 0 & 0 \\ -\frac{c_{aa}}{c_{ba}} & -\frac{c_{ab}}{c_{ba}} & -\frac{c_{bb}}{c_{ba}} & -\frac{c_{bc}}{c_{ba}} & 0 \\ 0 & 0 & 1 & 0 & 0 \\ \frac{-k_{lin}}{L} & 0 & 0 & 0 & \frac{-R}{L} \end{bmatrix}}_{\mathbf{A}} \begin{bmatrix} \dot{z} \\ z \\ F_r' \\ \int_{-\infty}^{t} F_r' \, d\tau \\ i \end{bmatrix} + \underbrace{\begin{bmatrix} 0 \\ 0 \\ 0 \\ 0 \\ \frac{1}{L} \end{bmatrix}}_{\mathbf{B}_u} \begin{bmatrix} v \end{bmatrix} + \underbrace{\begin{bmatrix} \frac{1}{mA} \\ 0 \\ 0 \\ 0 \\ 0 \end{bmatrix}}_{\mathbf{B}_v} \begin{bmatrix} F_e \end{bmatrix} \tag{2.73}$$

Repeating the same process for the output equations, we get

$$\begin{aligned} \dot{z} &= g_1 = \dot{z} \\ z &= g_2 = z \\ F_{pto} &= g_3 = k_{lin} i \\ i &= g_4 = i \\ v &= g_6 = v \end{aligned} \tag{2.74}$$

Arranging them in state-space, we get :

$$\begin{bmatrix} \dot{z} \\ z \\ F_{pto} \\ i \\ v \end{bmatrix} = \underbrace{\begin{bmatrix} 1 & 0 & 0 & 0 & 0 \\ 0 & 1 & 0 & 0 & 0 \\ 0 & 0 & 0 & 0 & k_{lin} \\ 0 & 0 & 0 & 0 & 1 \\ 0 & 0 & 0 & 0 & 0 \end{bmatrix}}_{\mathbf{C}} \begin{bmatrix} \dot{z} \\ z \\ F_r' \\ \int_{-\infty}^{t} F_r' \, d\tau \\ i \end{bmatrix} + \underbrace{\begin{bmatrix} 0 \\ 0 \\ 0 \\ 0 \\ 1 \end{bmatrix}}_{\mathbf{D}_u} \begin{bmatrix} v \end{bmatrix} + \underbrace{\begin{bmatrix} 0 \\ 0 \\ 0 \\ 0 \\ 0 \end{bmatrix}}_{\mathbf{D}_v} \begin{bmatrix} F_e \end{bmatrix} \tag{2.75}$$

Final input and output equations are :

$$\frac{d}{dt}\begin{bmatrix} \dot{z} \\ z \\ F_r' \\ \int_{-\infty}^{t} F_r'\, d\tau \\ i \end{bmatrix} = \underbrace{\begin{bmatrix} 0 & \frac{-k}{mA} & \frac{1}{mA} & 0 & \frac{k_{lin}}{mA} \\ 1 & 0 & 0 & 0 & 0 \\ -\frac{c_{aa}}{c_{ba}} & -\frac{c_{ab}}{c_{ba}} & -\frac{c_{bb}}{c_{ba}} & -\frac{c_{bc}}{c_{ba}} & 0 \\ 0 & 0 & 1 & 0 & 0 \\ \frac{-k_{lin}}{L} & 0 & 0 & 0 & \frac{-R}{L} \end{bmatrix}}_{\mathbf{A}} \begin{bmatrix} \dot{z} \\ z \\ F_r' \\ \int_{-\infty}^{t} F_r'\, d\tau \\ i \end{bmatrix} + \underbrace{\begin{bmatrix} 0 \\ 0 \\ 0 \\ 0 \\ \frac{1}{L} \end{bmatrix}}_{\mathbf{B}_u} \begin{bmatrix} v \end{bmatrix} + \underbrace{\begin{bmatrix} \frac{1}{mA} \\ 0 \\ 0 \\ 0 \\ 0 \end{bmatrix}}_{\mathbf{B}_v} \begin{bmatrix} F_e \end{bmatrix} \tag{2.76}$$

$$\begin{bmatrix} \dot{z} \\ z \\ F_{pto} \\ i \\ v \end{bmatrix} = \underbrace{\begin{bmatrix} 1 & 0 & 0 & 0 & 0 \\ 0 & 1 & 0 & 0 & 0 \\ 0 & 0 & 0 & 0 & k_{lin} \\ 0 & 0 & 0 & 0 & 1 \\ 0 & 0 & 0 & 0 & 0 \end{bmatrix}}_{\mathbf{C}} \begin{bmatrix} \dot{z} \\ z \\ F_r' \\ \int_{-\infty}^{t} F_r' \, d\tau \\ i \end{bmatrix} + \underbrace{\begin{bmatrix} 0 \\ 0 \\ 0 \\ 0 \\ 1 \end{bmatrix}}_{\mathbf{D}_u} \begin{bmatrix} v \end{bmatrix} + \underbrace{\begin{bmatrix} 0 \\ 0 \\ 0 \\ 0 \\ 0 \end{bmatrix}}_{\mathbf{D}_v} \begin{bmatrix} F_e \end{bmatrix} \tag{2.77}$$

2.6.1 Integrated model formulation with rate of change of current as a control input

In this case, rather than having voltages as an input, rate of change of current was modelled as a control input.

$$\frac{d}{dt}\begin{bmatrix} \dot{z} \\ z \\ F_r' \\ \int_{-\infty}^{t} F_r' \, d\tau \\ i \end{bmatrix}$$

$$= \underbrace{\begin{bmatrix} 0 & \frac{-k}{mA} & \frac{1}{mA} & 0 & \frac{k_{lin}}{mA} \\ 1 & 0 & 0 & 0 & 0 \\ -\frac{c_{aa}}{c_{ba}} & -\frac{c_{ab}}{c_{ba}} & -\frac{c_{bb}}{c_{ba}} & -\frac{c_{bc}}{c_{ba}} & 0 \\ 0 & 0 & 1 & 0 & 0 \\ 0 & 0 & 0 & 0 & 0 \end{bmatrix}}_{\mathbf{A}} \begin{bmatrix} \dot{z} \\ z \\ F_r' \\ \int_{-\infty}^{t} F_r' \, d\tau \\ i \end{bmatrix} + \underbrace{\begin{bmatrix} 0 \\ 0 \\ 0 \\ 0 \\ 1 \end{bmatrix}}_{\mathbf{B}_u} \begin{bmatrix} \frac{di}{dt} \end{bmatrix} + \underbrace{\begin{bmatrix} \frac{1}{mA} \\ 0 \\ 0 \\ 0 \\ 0 \end{bmatrix}}_{\mathbf{B}_v} \begin{bmatrix} F_e \end{bmatrix} \tag{2.78}$$

$$\begin{bmatrix} \dot{z} \\ z \\ F_{pto} \\ i \\ v \end{bmatrix} = \underbrace{\begin{bmatrix} 1 & 0 & 0 & 0 & 0 \\ 0 & 1 & 0 & 0 & 0 \\ 0 & 0 & 0 & 0 & k_{lin} \\ 0 & 0 & 0 & 0 & 1 \\ k_{lin} & 0 & 0 & 0 & R \end{bmatrix}}_{\mathbf{C}} \begin{bmatrix} \dot{z} \\ z \\ F_r' \\ \int_{-\infty}^{t} F_r' \, d\tau \\ i \end{bmatrix} + \underbrace{\begin{bmatrix} 0 \\ 0 \\ 0 \\ 0 \\ L \end{bmatrix}}_{\mathbf{D}_u} \left[\frac{di}{dt}\right] + \underbrace{\begin{bmatrix} 0 \\ 0 \\ 0 \\ 0 \\ 0 \end{bmatrix}}_{\mathbf{D}_v} \left[F_e\right] \tag{2.79}$$

Chapter 3: Control model development

In this section, a predictive model developed from the current time k to the horizon $k + Hp$ from [21] and [24] is discussed. The MPC formulation setup that was used in the simulation is summarized and the chapter ends with a brief discussion on convexity and the reason why one particular formulation of the models were chosen.

3.1 Sequential model setup

The sequential model first discussed in [32] and later developed in [21] solves forward in time and uses back substitution to find the future states.

$$\mathbf{x}(k+1) = \mathbf{A}\mathbf{x}(k) + \mathbf{B}_u\mathbf{u}(k) + \mathbf{B}_v\mathbf{v}(k) \tag{3.1}$$

$$\begin{aligned}
\mathbf{x}(k+2) &= \mathbf{A}\mathbf{x}(k+1) + \mathbf{B}_u\mathbf{u}(k+1) + \mathbf{B}_v\mathbf{v}(k+1) \\
&= \mathbf{A}(\mathbf{A}\mathbf{x}(k) + \mathbf{B}_u\mathbf{u}(k) + \mathbf{B}_v\mathbf{v}(k)) + \mathbf{B}_u\mathbf{u}(k+1) + \mathbf{B}_v\mathbf{v}(k+1) \\
&= \mathbf{A}^2\mathbf{x}(k) + [\mathbf{A}\mathbf{B}_u\mathbf{u}(k) + \mathbf{B}_u\mathbf{u}(k+1)] + [\mathbf{A}\mathbf{B}_v\mathbf{v}(k) + \mathbf{B}_v\mathbf{v}(k+1)]
\end{aligned} \tag{3.2}$$

$$\begin{aligned} \mathbf{x} &\in \Re^{n_x \times 1} \\ \mathbf{u} &\in \Re^{n_u \times 1} \\ \mathbf{v} &\in \Re^{n_v \times 1} \\ \mathbf{A} &\in \Re^{n_x \times n_x} \\ \mathbf{B}_u &\in \Re^{n_x \times n_u} \\ \mathbf{B}_v &\in \Re^{n_x \times n_v} \end{aligned} \tag{3.3}$$

$$\mathbf{y}(k) = \mathbf{C}\mathbf{x}(k) + \mathbf{D}_u\mathbf{u}(k) + \mathbf{D}_v\mathbf{v}(k) \tag{3.4}$$

Based on this formulation a set of predictive values are developed for the outputs. output and not a state.

The prediction model for the outputs developed in [21] is used for both versions of the integrated-generator model developed in this research.

$$\begin{aligned} \mathbf{y} &\in \Re^{n_y \times 1} \\ \mathbf{C} &\in \Re^{n_y \times n_x} \\ \mathbf{D}_u &\in \Re^{n_y \times n_u} \\ \mathbf{D}_v &\in \Re^{n_y \times n_v} \end{aligned} \tag{3.5}$$

$$\begin{aligned} \mathbf{y}(k+1) &= \mathbf{C}(\mathbf{A}\mathbf{x}(k) + \mathbf{B}_u\mathbf{u}(k) + \mathbf{B}_v\mathbf{v}(k)) + \mathbf{D}_u\mathbf{u}(k+1) + \mathbf{D}_v\mathbf{v}(k+1) \\ &= \mathbf{C}\mathbf{A}\mathbf{x}(k) \\ &\quad + \mathbf{C}\mathbf{B}_u\mathbf{u}(k) + \mathbf{D}_u\mathbf{u}(k+1) \\ &\quad + \mathbf{C}\mathbf{B}_v\mathbf{v}(k) + \mathbf{D}_v\mathbf{v}(k+1) \end{aligned} \tag{3.6}$$

$$
\begin{aligned}
\mathbf{y}(k+2) &= \mathbf{CA}^2\mathbf{x}(k) \\
&\quad + \mathbf{CAB}_u\mathbf{u}(k) + \mathbf{CB}_u\mathbf{u}(k+1) \\
&\quad + \mathbf{CAB}_v\mathbf{v}(k)) + \mathbf{CB}_v\mathbf{v}(k+1) \\
&\quad + \mathbf{D}_u\mathbf{u}(k+2) + \mathbf{D}_v\mathbf{v}(k+2) \\
&= \mathbf{CA}^2\mathbf{x}(k) \\
&\quad + \mathbf{CAB}_u\mathbf{u}(k) + \mathbf{CB}_u\mathbf{u}(k+1) + \mathbf{D}_u\mathbf{u}(k+2) \\
&\quad + \mathbf{CAB}_v\mathbf{v}(k)) + \mathbf{CB}_v\mathbf{v}(k+1) + \mathbf{D}_v\mathbf{v}(k+2)
\end{aligned}
\tag{3.7}
$$

The prediction horizon is H_p. A general rule of thumb is to use a prediction horizon of 10 seconds.

$$
\underbrace{\begin{bmatrix} \mathbf{y}(k) \\ \mathbf{y}(k+1) \\ \mathbf{y}(k+2) \\ \mathbf{y}(k+3) \\ \vdots \\ \mathbf{y}(k+H_p) \end{bmatrix}}_{\vec{\mathbf{y}}(k)} = \underbrace{\begin{bmatrix} \mathbf{C} \\ \mathbf{CA} \\ \mathbf{CA}^2 \\ \mathbf{CA}^3 \\ \vdots \\ \mathbf{CA}^{H_p} \end{bmatrix}}_{\mathbf{S}_x} \mathbf{x}(k)
$$

$$
+ \underbrace{\begin{bmatrix} \mathbf{D}_u & 0 & 0 & 0 & \cdots & 0 \\ \mathbf{CB}_u & \mathbf{D}_u & 0 & 0 & \cdots & 0 \\ \mathbf{CAB}_u & \mathbf{CB}_u & \mathbf{D}_u & 0 & \cdots & 0 \\ \mathbf{CA}^2\mathbf{B}_u & \mathbf{CAB}_u & \mathbf{CB}_u & \mathbf{D}_u & \cdots & 0 \\ \vdots & \vdots & \vdots & \vdots & \ddots & \vdots \\ \mathbf{CA}^{H_p-1}\mathbf{B}_u & \mathbf{CA}^{H_p-2}\mathbf{B}_u & \cdots & \cdots & \mathbf{CB}_u & \mathbf{D}_u \end{bmatrix}}_{\mathbf{S}_u} \underbrace{\begin{bmatrix} \mathbf{u}(k) \\ \mathbf{u}(k+1) \\ \mathbf{u}(k+2) \\ \mathbf{u}(k+3) \\ \vdots \\ \mathbf{u}(k+H_p) \end{bmatrix}}_{\vec{\mathbf{u}}(k)}
$$

$$
+ \underbrace{\begin{bmatrix} \mathbf{D}_v & 0 & 0 & 0 & \cdots & 0 \\ \mathbf{CB}_v & \mathbf{D}_v & 0 & 0 & \cdots & 0 \\ \mathbf{CAB}_v & \mathbf{CB}_v & \mathbf{D}_v & 0 & \cdots & 0 \\ \mathbf{CA}^2\mathbf{B}_v & \mathbf{CAB}_v & \mathbf{CB}_u & \mathbf{D}_v & \cdots & 0 \\ \vdots & \vdots & \vdots & \vdots & \ddots & \vdots \\ \mathbf{CA}^{H_p-1}\mathbf{B}_v & \mathbf{CA}^{H_p-2}\mathbf{B}_v & \cdots & \cdots & \mathbf{CB}_v & \mathbf{D}_v \end{bmatrix}}_{\mathbf{S}_v} \underbrace{\begin{bmatrix} \mathbf{v}(k) \\ \mathbf{v}(k+1) \\ \mathbf{v}(k+2) \\ \mathbf{v}(k+3) \\ \vdots \\ \mathbf{v}(k+H_p) \end{bmatrix}}_{\vec{\mathbf{v}}(k)} \tag{3.8}
$$

For the dq model, as linearization was done, the value of the disturbance matrices in the prediction formulation is not zero. For the DC model however, the model was linear and so only the excitation force is the disturbance.

3.2 Excitation force prediction

For the excitation force prediction, an adaptive least squares regression model was used that was developed in [24]. This was further extended to also predict other disturbance components present in the model.

$$F_e(k+1|k) = \alpha_1 F_e(k) + \alpha_2 F_e(k-1) + ... + \alpha_n F_e(k-n+1) \tag{3.9}$$

$$F_e(k+2|k) = \alpha_1 F_e(k+1|k) + \alpha_2 F_e(k) + ... + \alpha_n F_e(k-n+2) \tag{3.10}$$

$$F_e(k+Hp|k) = \alpha_1 F_e(k+Hp-1|k) + \alpha_2 F_e(k+Hp-2|k) + ... + \alpha_n F_e(k+Hp-n|k) \tag{3.11}$$

Here, based on the previous value of F_e, the next value is predicted [24].

3.3 Optimization function

The crucial part of the MPC formulation is the optimization function where the goal is to capture maximum power while respecting a set of constraints. This problem is generally reformulated as a minimization problem as per [33]. In both cases of the integrated generator model, the product of voltage times current i.e. the electrical power is being minimized. A general form of the minimization function according to [24] is :

$$\min J(x) = \frac{1}{2}x^T Hx + f^T x \tag{3.12}$$

Subject to

$$Ax \leq b \tag{3.13}$$

MATLAB's quadratic programming algorithm solves for the best value of inputs that minimizes the above function. In this case, based on the generator formulation used, it can be the ideal values of d and q voltages for the dq model, the voltage for the DC model or the rate of change of current if the control input is in terms of rate of change of current that results in the most negative power which will equivalently be the most positive power.

The format of MATLAB's quadprog is :

$$\overrightarrow{\mathbf{y}}(k) = \mathbf{S}_x\mathbf{x}(k) + \mathbf{S}_u\overrightarrow{\mathbf{u}}(k) + \mathbf{S}_v\overrightarrow{\mathbf{v}}(k) \tag{3.14}$$

$$J(k) = \frac{1}{2}\overrightarrow{\mathbf{y}}(k)^T\mathbf{Q}\overrightarrow{\mathbf{y}}(k) + \frac{1}{2}\overrightarrow{\mathbf{u}}(k)^T\mathbf{R}\overrightarrow{\mathbf{u}}(k) \tag{3.15}$$

Here in case of both the integrated generator models used, the Q matrix sub-selects the values of voltage and currents and the MPC controller solves for optimal values of voltages that will minimize the product of voltage times current i.e. electrical power.

3.4 Convexity

The challenge when using a control scheme like MPC is that the problem is usually non-convex. In this section, the problem is convex if eigen values of the hessian are positive i.e. the hessian is positive semi-definite. A more detailed approach of how this is formulated was explored in [34]. In the integrated generator formulation, sub-selection of voltages and currents is done based on the cost matrix formulation but, there is a penalty for the power generated.

$$J(k) = \frac{1}{2}\overrightarrow{\mathbf{u}}(k)^T\underbrace{(\mathbf{S_u}^T\mathbf{Q}\mathbf{S_u} + \mathbf{R})}_{\mathbf{H}}\overrightarrow{\mathbf{u}}(k) + \overrightarrow{\mathbf{u}}(k)^T\underbrace{\mathbf{S_u}^T\mathbf{Q}(\mathbf{S_x}\mathbf{x}(k) + \mathbf{S_v}\overrightarrow{\mathbf{v}}(k))}_{\boldsymbol{f}} \tag{3.16}$$

During this sub-selection however, integrating the generator with the hydrodynamic model made the problem more non-convex. This meant that to make the problem convex, precise selection of the matrix that denotes cost for control action which in this formulation will be the matrix $\mathbf{R}$ was required and this is tricky as the more penalty there is for the '*vi*' sub-selection, cost for power electronics. To illustrate this, the minimum eigen values and their variation with resistance and back-emf constant in case of the DC model is illustrated for two types of formulation in the upcoming sections.

3.4.1 Non-positive semidefiniteness for di/dt formulation of DC model

In this case, the control inputs were rate of change of current for the DC machine. A range of winding resistances and back emf constants were chosen. For each possible combination, the hessian was formulated and the minimum eigen value of the hessian was calculated. These were then plotted to see the variation of resistance and emf constants with the eigen values.

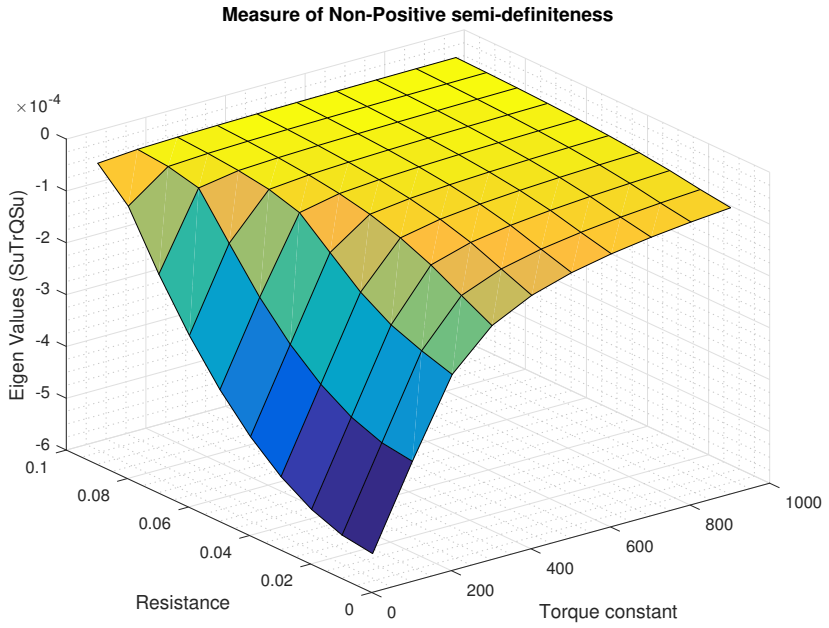

Figure 3.1: Measure of non-positive semi-definiteness. Case : 1

From the above figure, it is evident that the higher the torque of the machine is, the more closer it is to convexity but there seems to be a trade off here as the winding resistance is also linked to the convexity and the challenging part here is that higher winding resistance leads to more losses. So, a careful selection of both

these parameters is required.

3.4.2 Non-positive semidefiniteness for v formulation of DC model

The control formulation becomes even more challenging when the formulation was done using voltages as the control input. The variation of resistance and emf constant with the eigen values is much more erratic as in Fig 3.2. It is interesting to note that the scale of eigen values are much larger in this formulation. So, to get closer to convexity, higher values of winding resistances are required and this would increase the penalty for control action and also the losses.

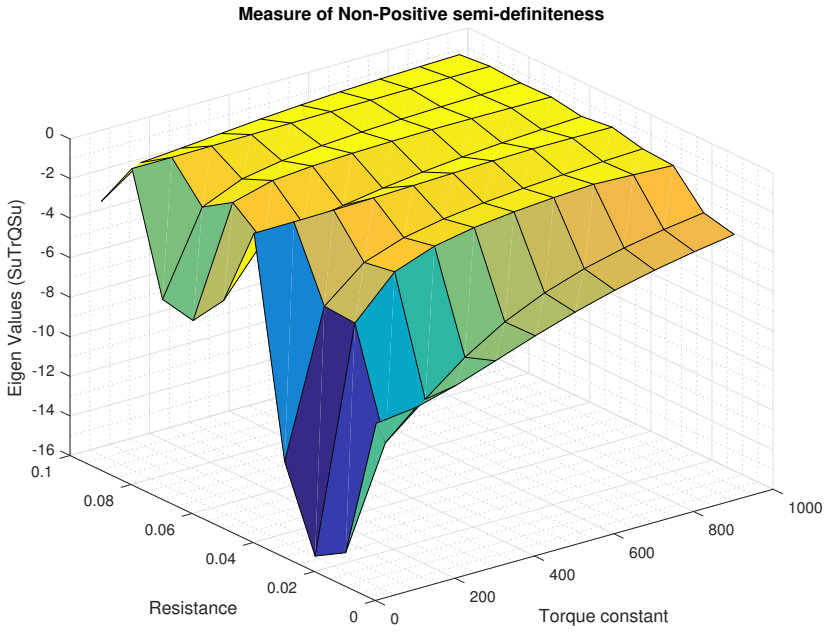

Figure 3.2: Measure of non-positive semi-definiteness. Case : 2

In this case, selecting an ideal resistance and emf constant to get to a convex formulation is much more challenging as the variation w.r.t. eigen values are vastly different for both methods. Based on these results, case 1 was chosen and modeled using Simulink. Tuning the penalty matrices is challenging as precise selection was required since these components directly impact stability of the model. Several methods like Cholesky decomposition to remove the negative eigen values from the hessian, adding a positive offset based on incrementing the negative minimum eigen value by one-five percent were attempted but these seemed to result in a lot more reactive power along with extremely high buoy position and velocity. So, the penalty matrix was made significantly larger based on some manual tuning to make sure that the model was stable.

Chapter 4: Simulation and results

4.1 Integrated DC generator model

In this section, the formulation w.r.t. di/dt as the control inputs were modelled using Simulink for both the generator models. One for a simple DC machine and the other for a AC generator.

4.1.1 Modelling in simulink for integrated generator model

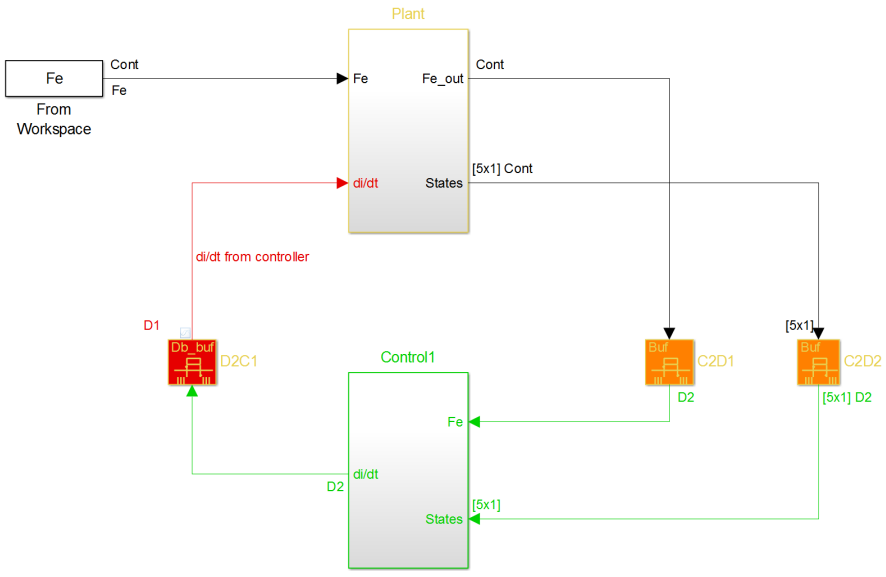

Figure 4.1: Integrated DC generator system model

This system was modeled as per equation 2.78 and equation 2.79. The excitation force data and the rate of change of current are inputs to the plant model. The controller takes in excitation forces and states in discreet time domain and builds a predictive model for the excitation forces based on the adaptive least squares regression method that was discussed in the previous chapter.

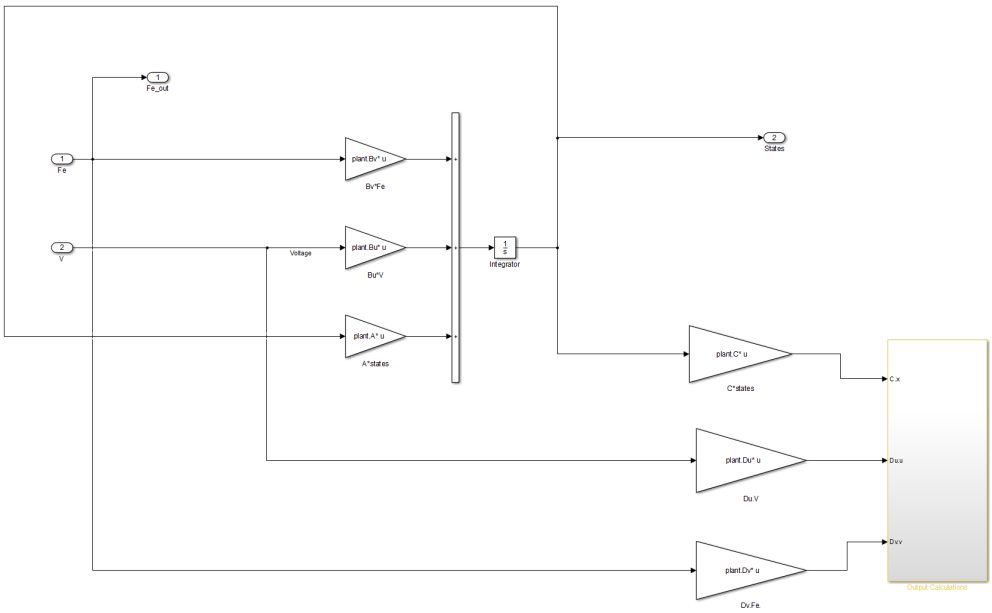

Figure 4.2: State-space DC generator plant model

Here, output set of equations that were defined in 2.79 are used to calculate the buoy position, velocity, take-off force, voltage and current.

The optimization algorithm of MPC gives us a vector of output voltages that goes from the current time step to 20 samples ahead in the future. However, the plant model requires information about only the voltage that needs to be applied at the current time step. Additionally, the MPC function block is also giving us

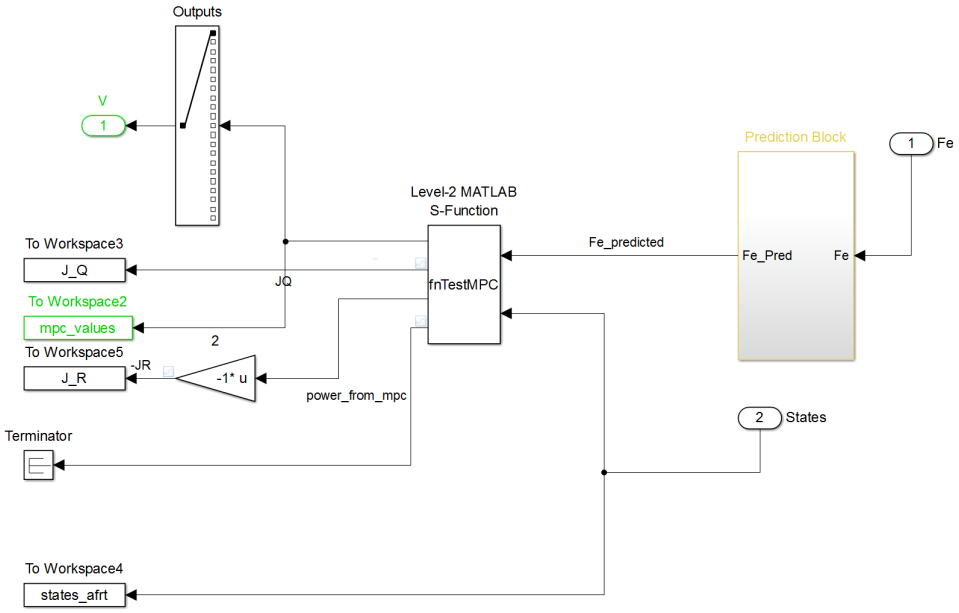

Figure 4.3: Controller view

information about how much the controller is being utilized. The results of all these parameters are discussed in the upcoming sections.

4.1.2 Results for integrated DC generator model (Unconstrained)

In this case, no constraints were placed on the controller. The cost matrix was tuned to a value to make sure the buoy position and velocity were marginally above $2m$ and $1.5m/s$. The value was chosen as the negative minimum of the hessian incremented by a factor of $7.7 * 10^3$. The reason why this particular value was chosen is because values above this show a large amount of reactive power being fed back into the ocean.

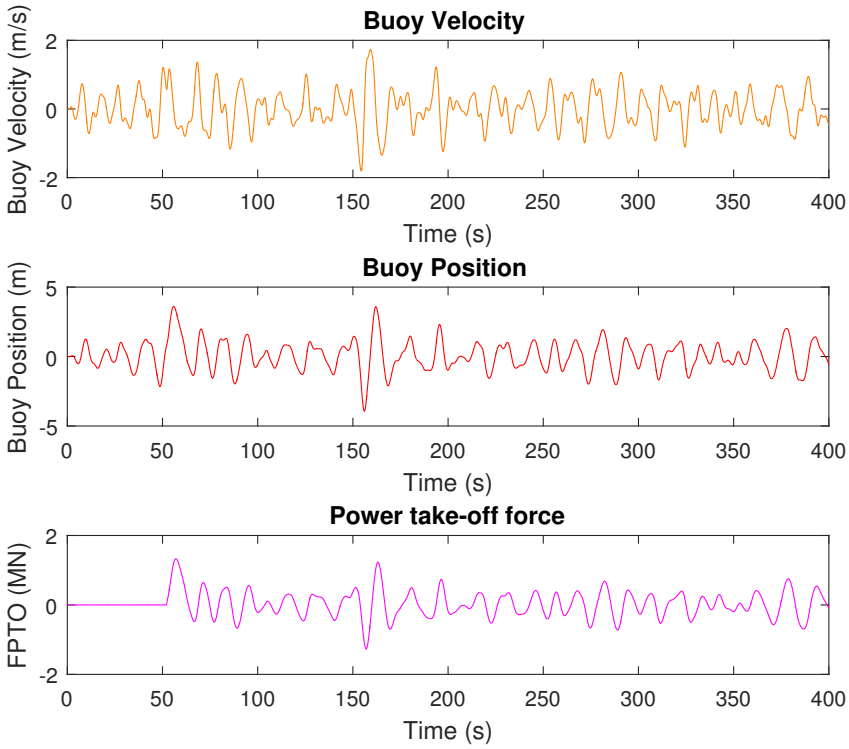

Figure 4.4: Buoy velocity, position, PTO force for integrated DC-generator (unconstrained)

The buoy position is over $2m$ at a few points due to the lack of constraints. Similar to the position plot, the buoy velocity goes over the permissible constraints at a few points. PTO force however, seems to be reasonable in the unconstrained case. However, the force would reduce significantly upon constraining the position and velocity.

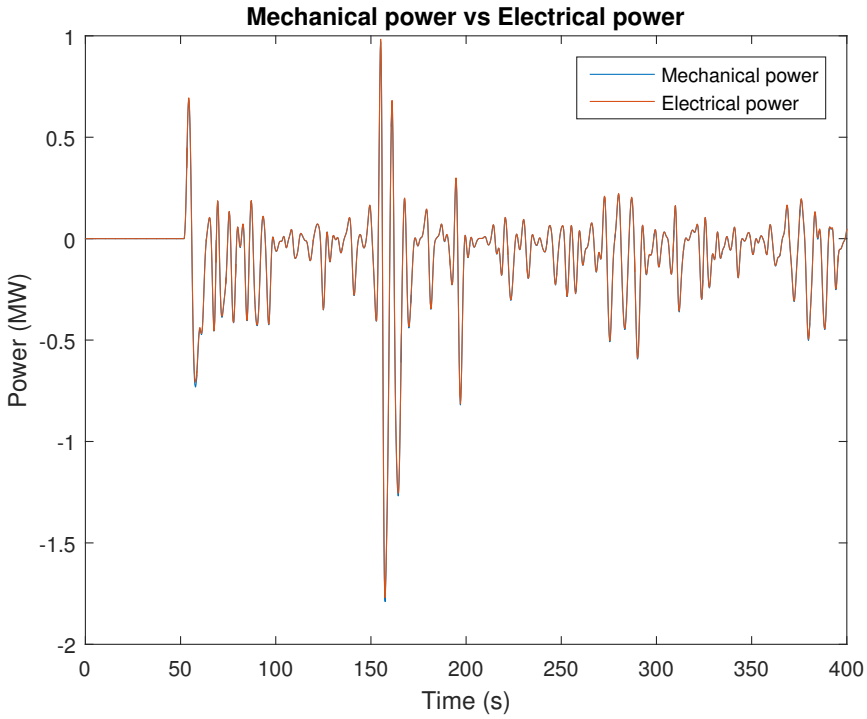

Figure 4.5: Electrical and mechanical power for integrated DC-generator (unconstrained)

In this formulation, the electrical efficiency (electrical power/mechanical power) is 97.27%. This is shown in Fig 4.5 by putting the electrical and mechanical power plots on top of each other. The remaining power is lost as heat and this is shown in Fig 4.6.

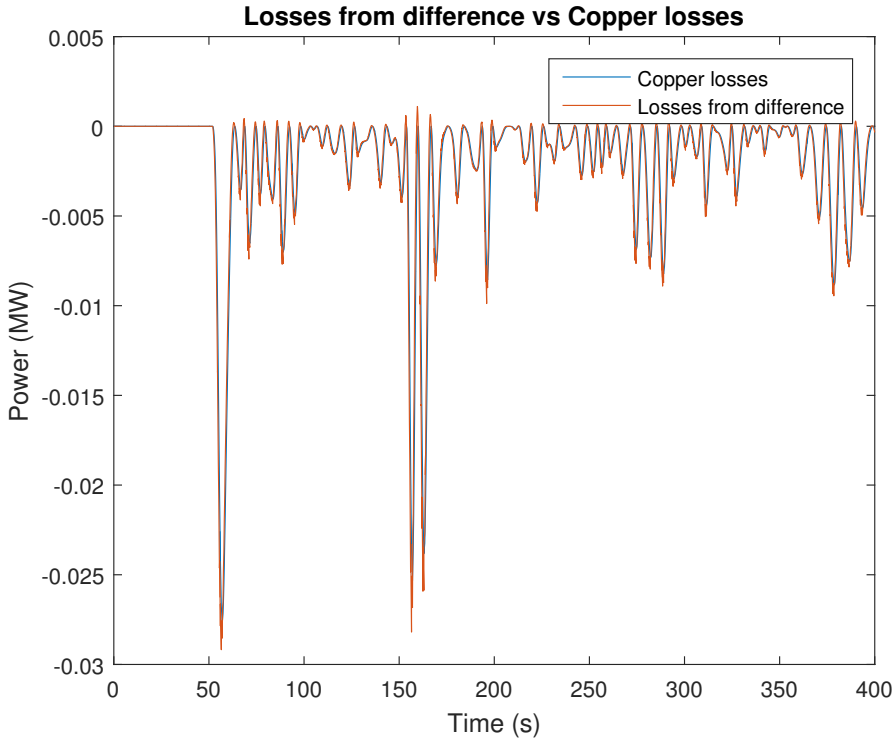

Figure 4.6: Losses for integrated DC-generator (unconstrained)

To check if all the losses are copper losses, we compare the difference between the mechanical and electrical power with the I^2R losses. They are on top of each other which confirms that all the losses are heat.

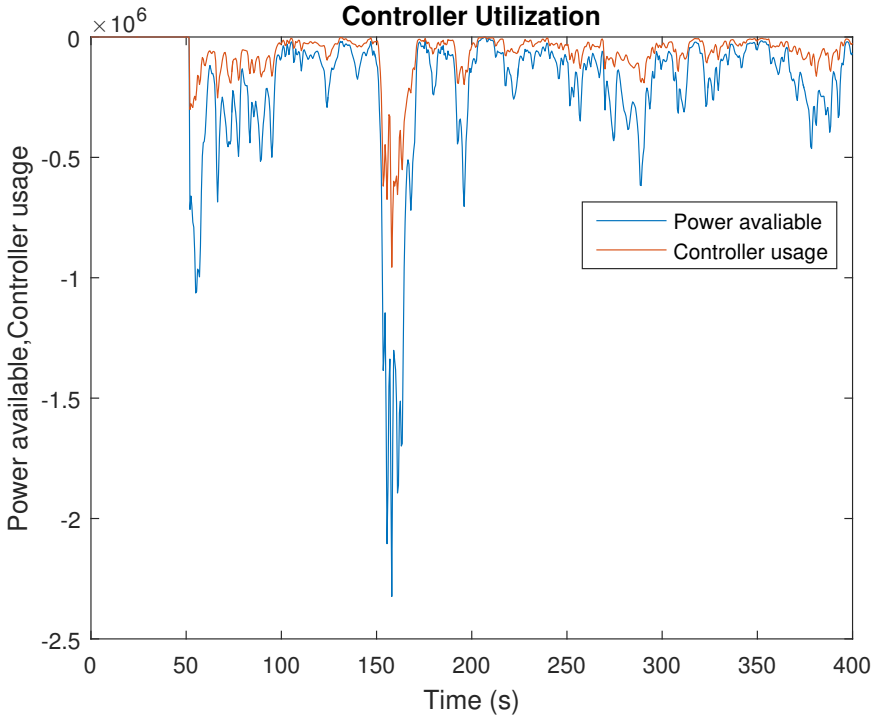

Figure 4.7: Controller utilization for integrated DC-generator (unconstrained)

The amount of utilization of the controller is shown in Fig 4.7. It is interesting to note that even without constraints, the controller isn't utilized to its maximum potential at the 150 second mark. This could be due to the fact the optimization algorithm doesn't see it as a viable choice to capture all the available power as it would increase the amount of power being put back into the ocean.

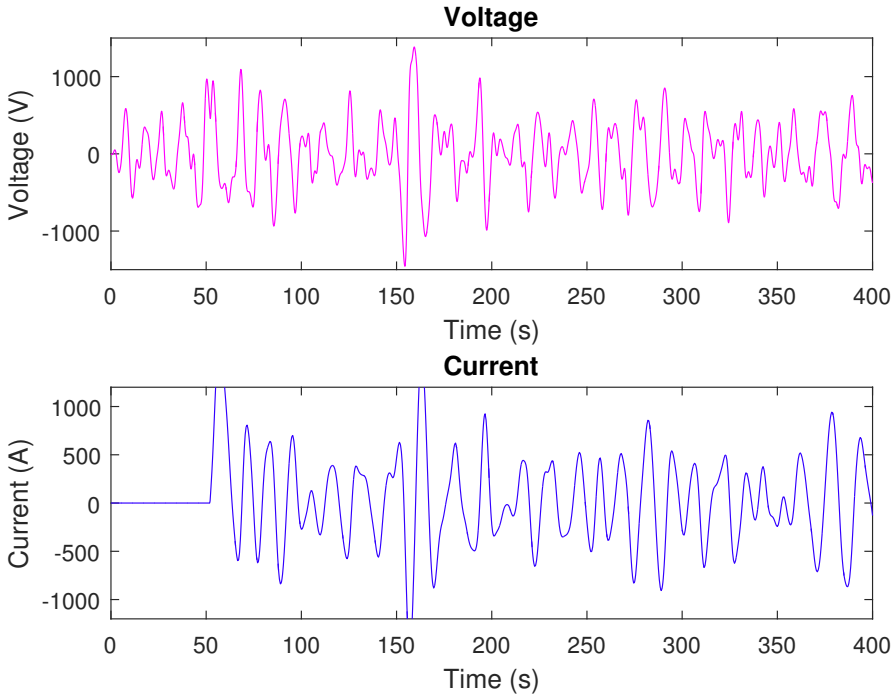

Figure 4.8: Voltage and current waveforms for integrated DC-generator (unconstrained)

From the above plots for voltages and currents, this formulation seems to work really well for small-scale WECs as the idea is to constrain the voltage at 1200 V and the current at 1000 A.

4.1.3 Results for integrated DC generator model (Constrained)

The following constraints were chosen for this f.

- Buoy position : $2m$

- Buoy velocity : 1.5 m/s
- Fpto : $6 * 10^8$ N
- Voltage : 1200 V
- Current : 1000 A

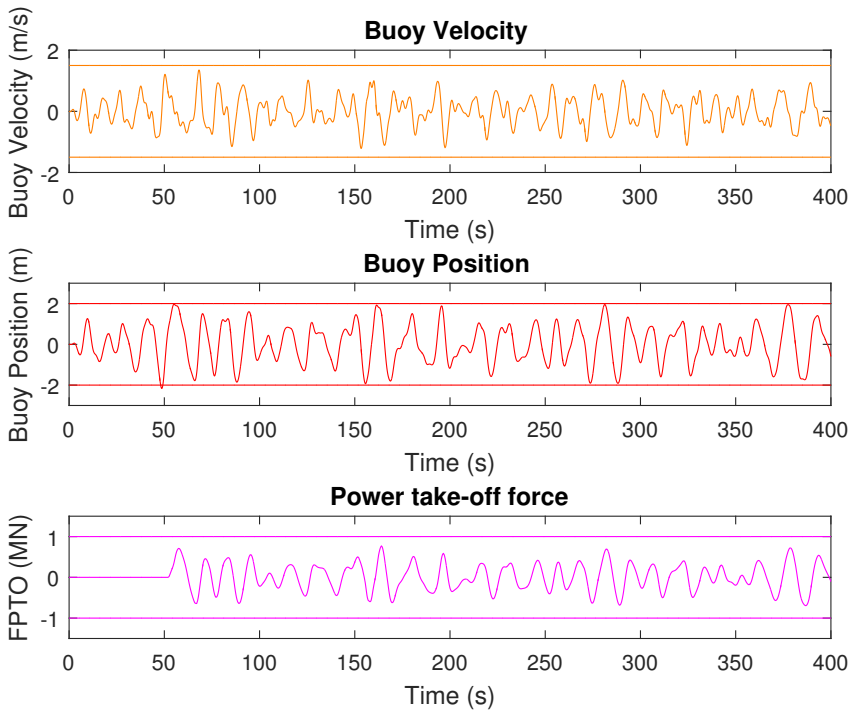

Figure 4.9: Buoy velocity, position, PTO force for integrated DC-generator (Constrained)

The model's behavior under constraints on all the outputs is show in Fig 4.9. As expected, there is a significant drop in the PTO force due to position and velocity being constrained.

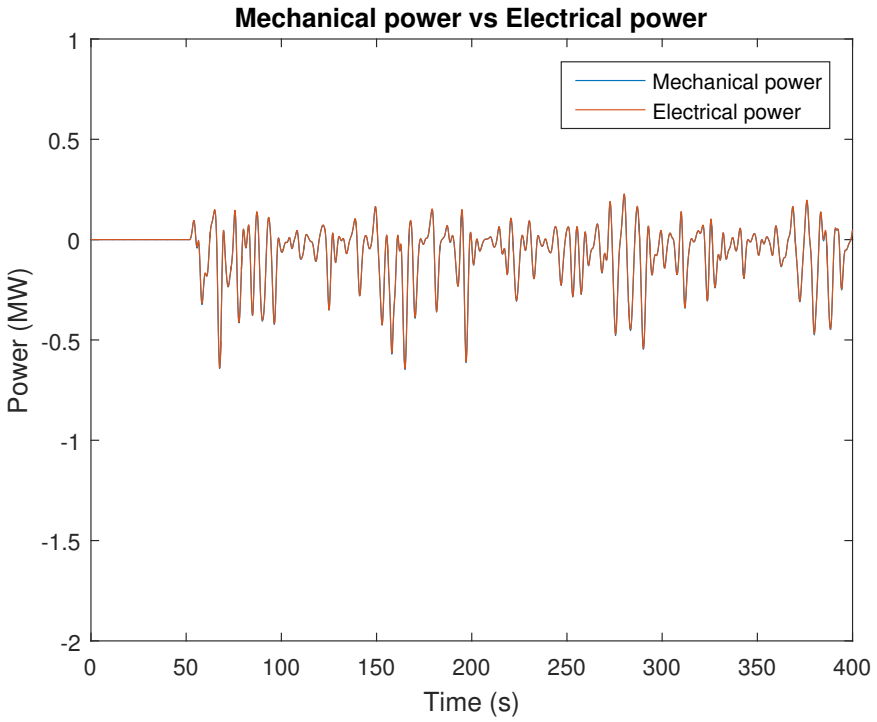

Figure 4.10: Electrical and Mechanical power for Integrated DC-generator (Constrained)

In this case, there is a significant drop in power due to the constraints applied. However, the efficiency is close to 98 percent and the peak power is close to 0.7 MW.

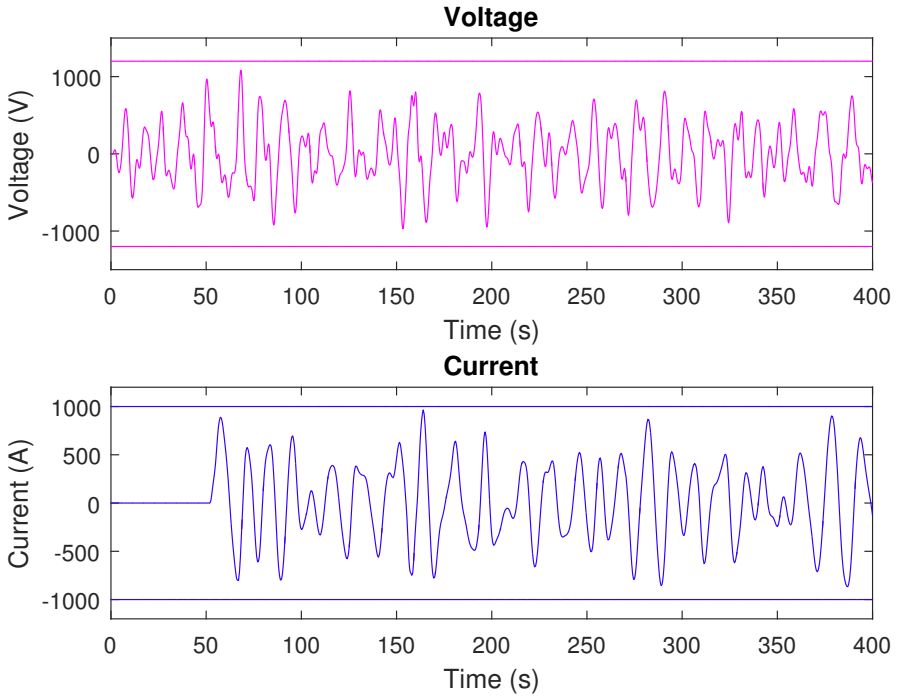

Figure 4.11: Voltage and current waveforms for integrated DC-generator (Constrained)

The voltage and current are well below the applied constraints as seen from the above Fig 4.11.

4.2 Integrated AC generator model

In this section, the di/dt method of formulation is used in integration of a AC generator model into a state-space hydrodynamic model.

4.2.1 Modelling in simulink for AC generator

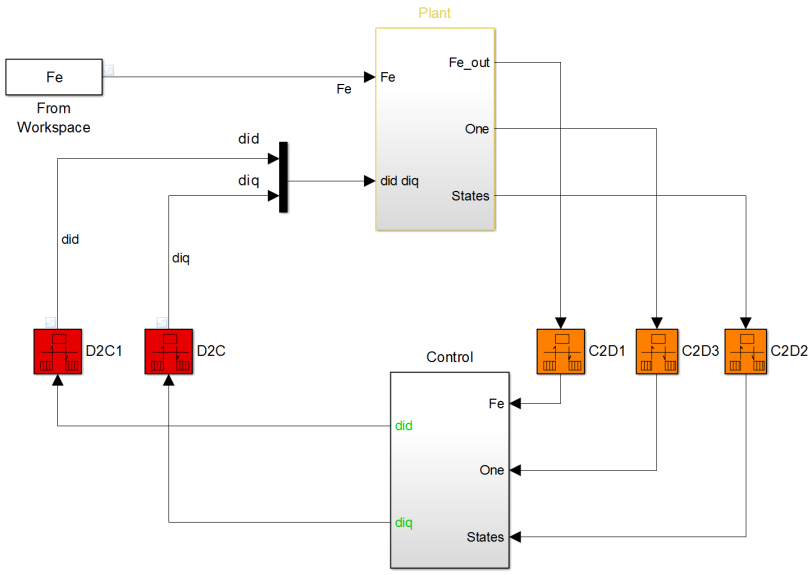

Figure 4.12: Integrated AC generator system model

The modelling scheme is very similar to that of the DC generator as seen from Fig 4.12. The models are based on equations 2.68 and 2.69. Initially, all the linearization points were set to zero.

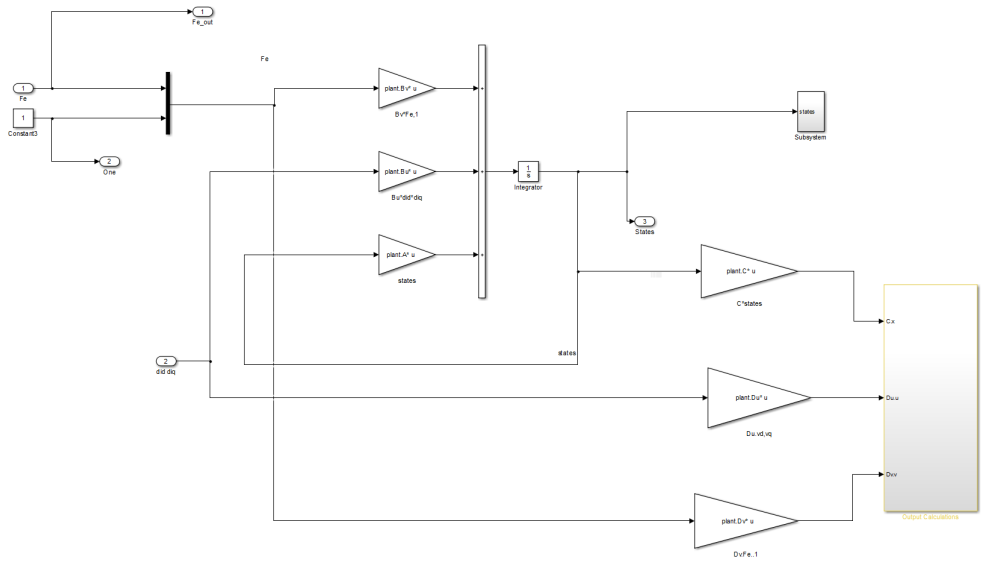

Figure 4.13: State-space plant model for AC generator

In this version of the model, as the equations were linearized, there are some disturbance components that show up in the formulation. The outputs in this case are buoy position, velocity,power take-off force, d/q axes voltages and currents.

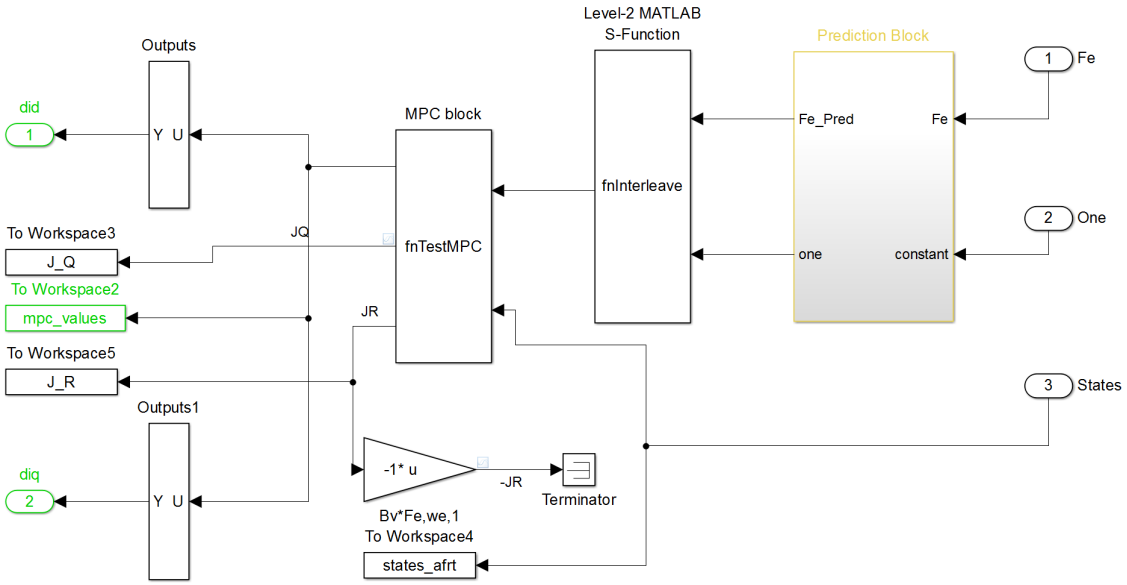

Figure 4.14: Controller view

The controller formulation is slightly different in this case. There are two disturbance predictions. Along with this, there is also an interleaving block that uses Matlab's reshape functionality to make sure the predictions line up on top of each other according to the prediction horizon i.e. excitation force prediction at sample k followed by prediction for one at sample k ; this is followed by the same for samples k+1,k+2 and so on.

4.2.2 Results for integrated AC generator model (Unconstrained)

The dq model was allowed to run unconstrained but the cost matrix was tuned so that the amount of power being put into the ocean (i.e. the reactive power) was not dominating the amount of power produced.

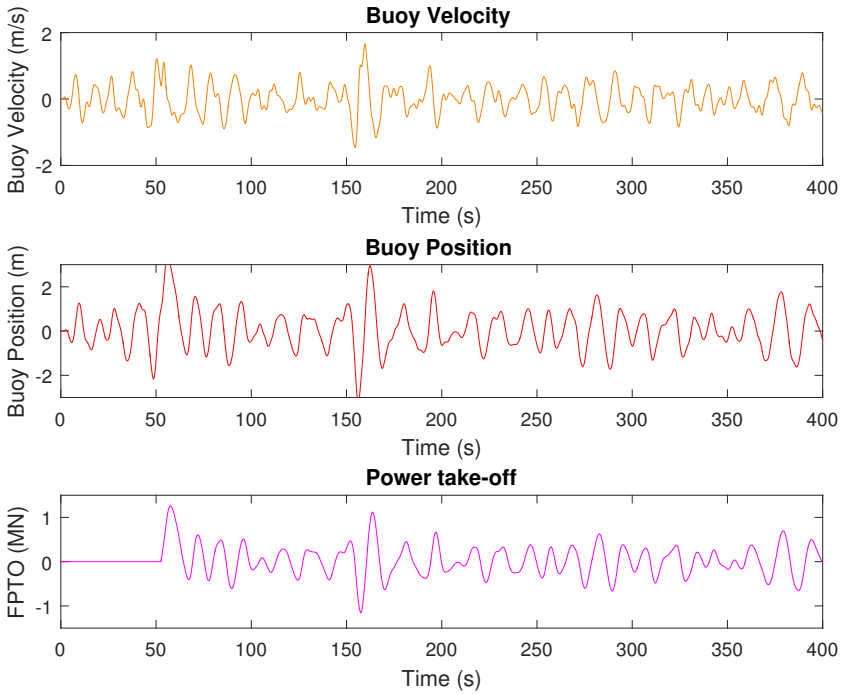

Figure 4.15: Buoy velocity, position, PTO force for the Integrated AC generator (unconstrained)

In this case, the buoy velocity and position are slightly above the expected range due to the lack of constraints. It is possible to relax the cost matrices even more to get more power but this would mean more losses and more reactive power.

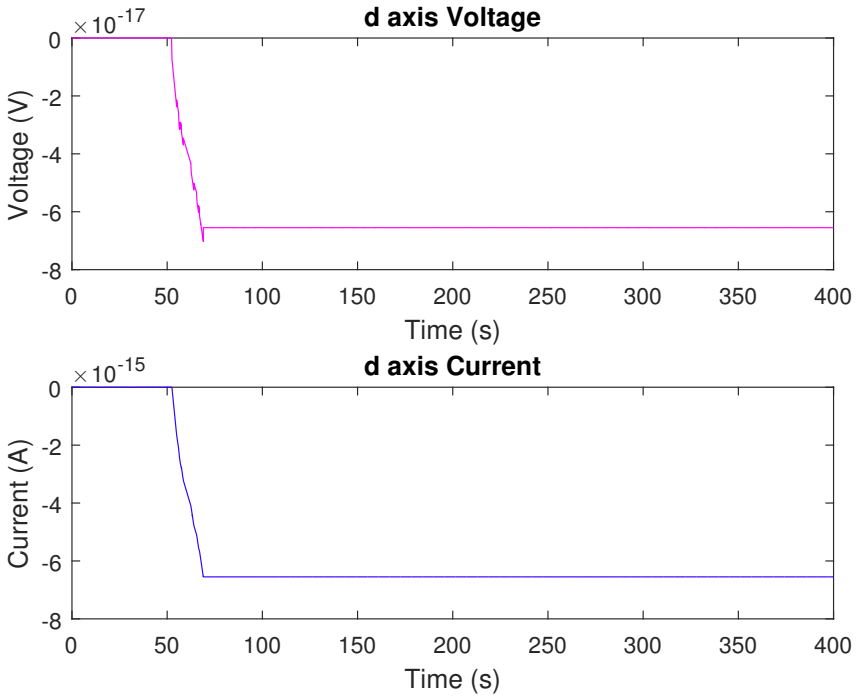

Figure 4.16: d axis voltage and current waveforms for integrated AC generator (unconstrained)

Since the linearization points are set to zero, the d axis voltages and currents are close to zero in this case. The system behavior will be very close to the DC version of the model.

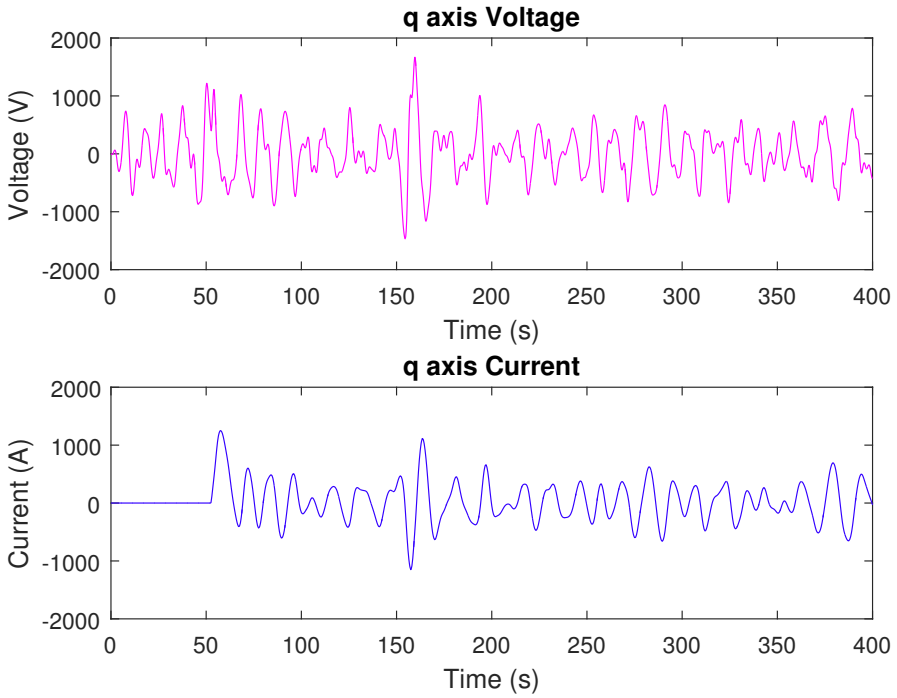

Figure 4.17: q axis voltage and current waveforms for integrated AC generator (unconstrained)

The q axis voltages and currents however are allowed to slightly go over the constraints to maintain a balance between the losses incurred and the reactive power given back to the ocean.

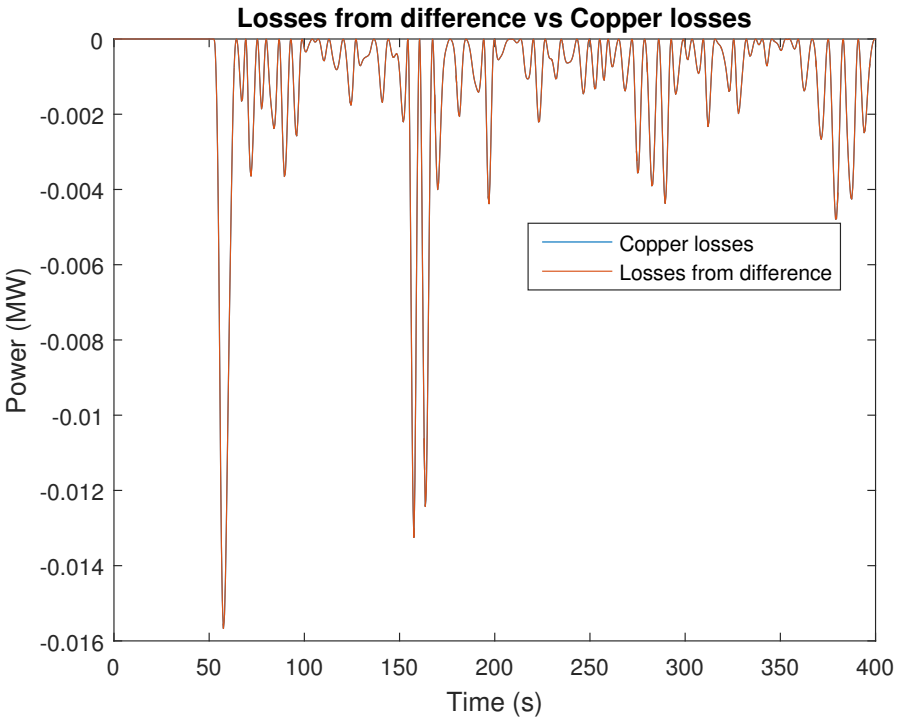

Figure 4.18: Losses for integrated AC generator (unconstrained)

The check for losses is done in this case as well to see if all the losses are copper losses and from Fig 4.18, that seems to be the case. In this formulation, the losses were calculated as $i_d^2R + i_q^2R$ but since the d axis current was close to zero, the losses are predominantly i_q^2R.

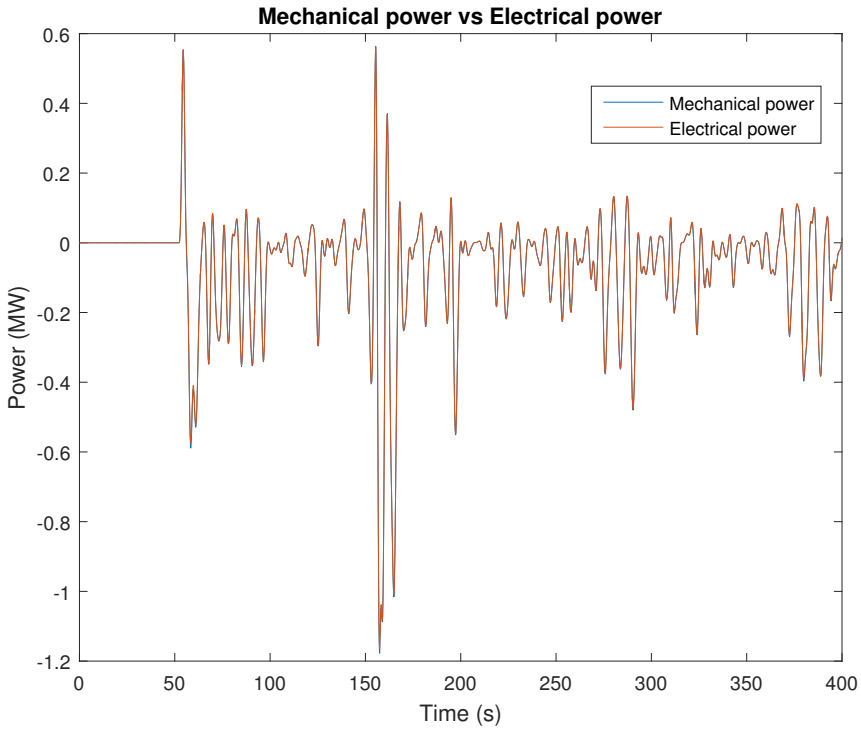

Figure 4.19: Electrical and mechanical power for integrated AC generator model (unconstrained)

In this case, the electrical machine efficiency was close to 98%. It is important to note that while higher power generation is possible, it becomes increasing difficult to tune the controller once constraints are applied. This could result in a significant amount of in-feasibility catches when running the simulation model as the controller is forced to go beyond constraints at several points.

4.2.3 Results for integrated AC generator model (Constrained)

The dq model was allowed to run with constraints and the cost matrices were tuned accordingly.

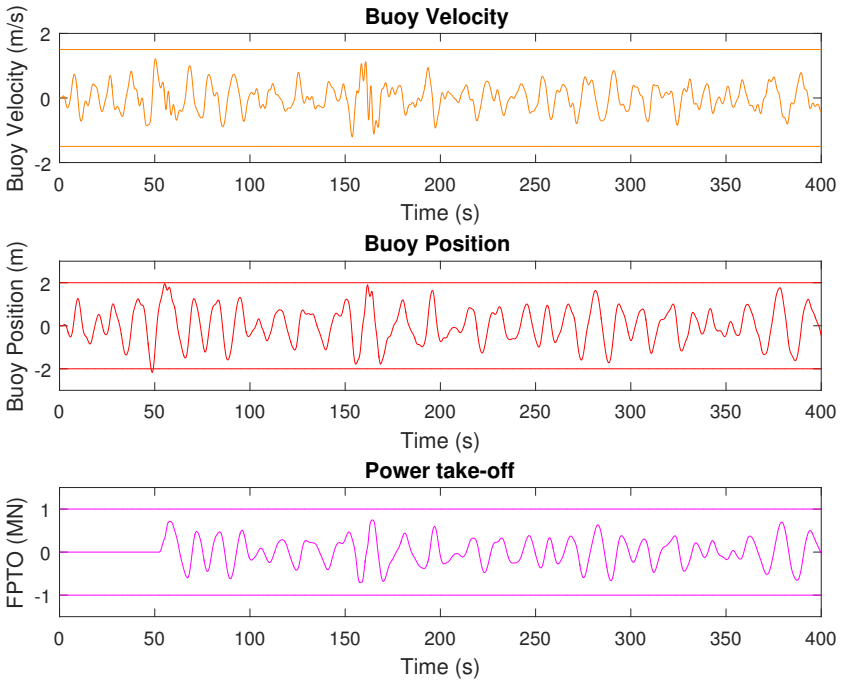

Figure 4.20: Buoy velocity, position, PTO force for the Integrated AC generator (constrained)

In this case, the buoy velocity and position are well under the set constraints.

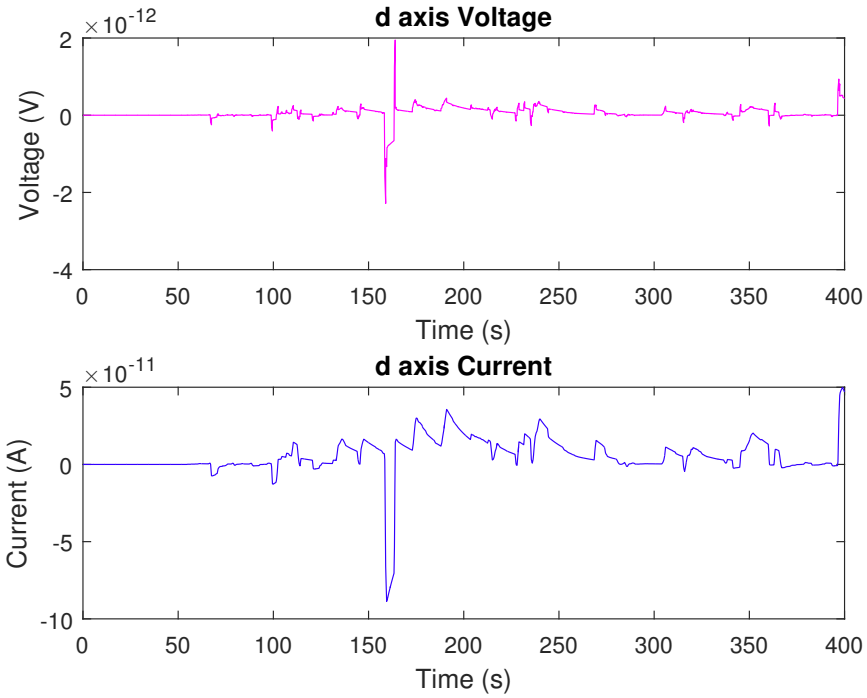

Figure 4.21: d axis voltage and current waveforms for integrated AC generator (constrained)

Since the linearization points are set to zero, the d axis voltages and currents are close to zero in this case. The system behavior will be very close to the DC version of the model.

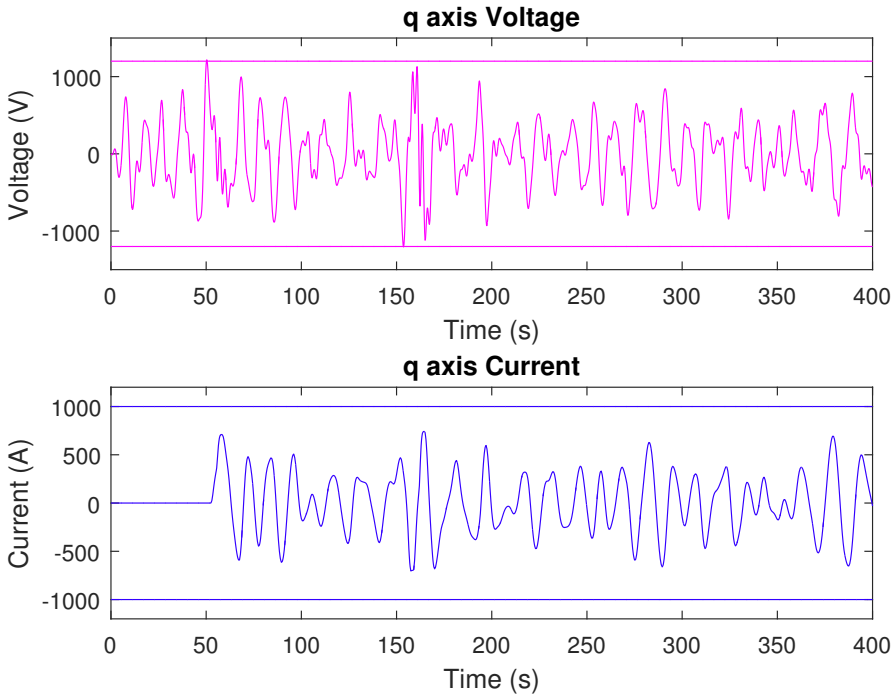

Figure 4.22: q axis voltage and current waveforms for integrated AC generator (constrained)

The q axis voltages and currents are well constrained. It is possible to relax the constraints slightly but since this is linked to position and velocity, a balance is needed.

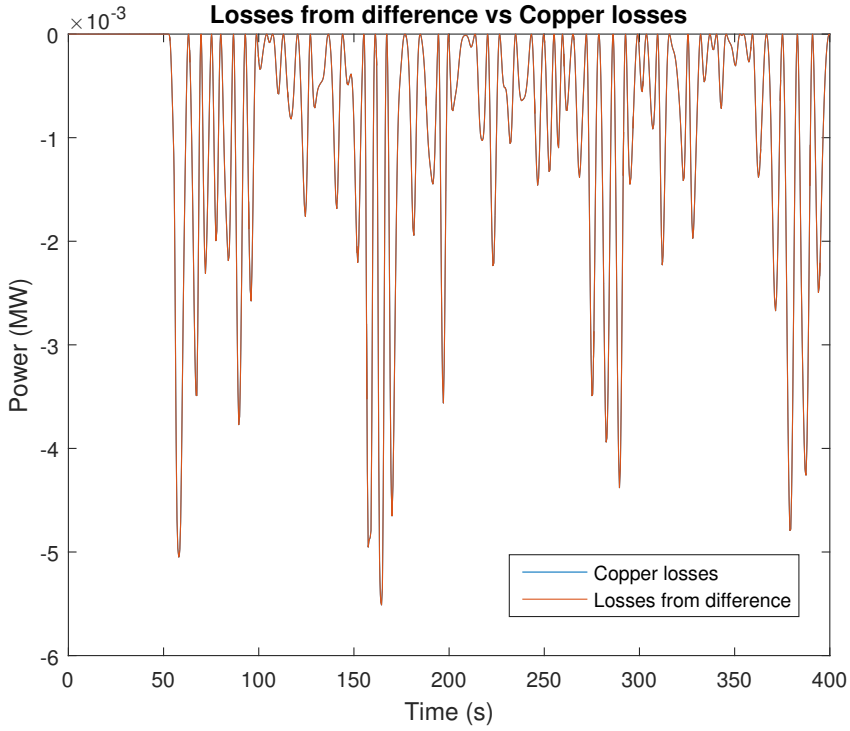

Figure 4.23: Losses for integrated AC generator (constrained)

Similar to the previous case, the losses were calculated as $i_d^2R + i_q^2R$ but since the d axis current was negligible, the losses are predominantly i_q^2R.

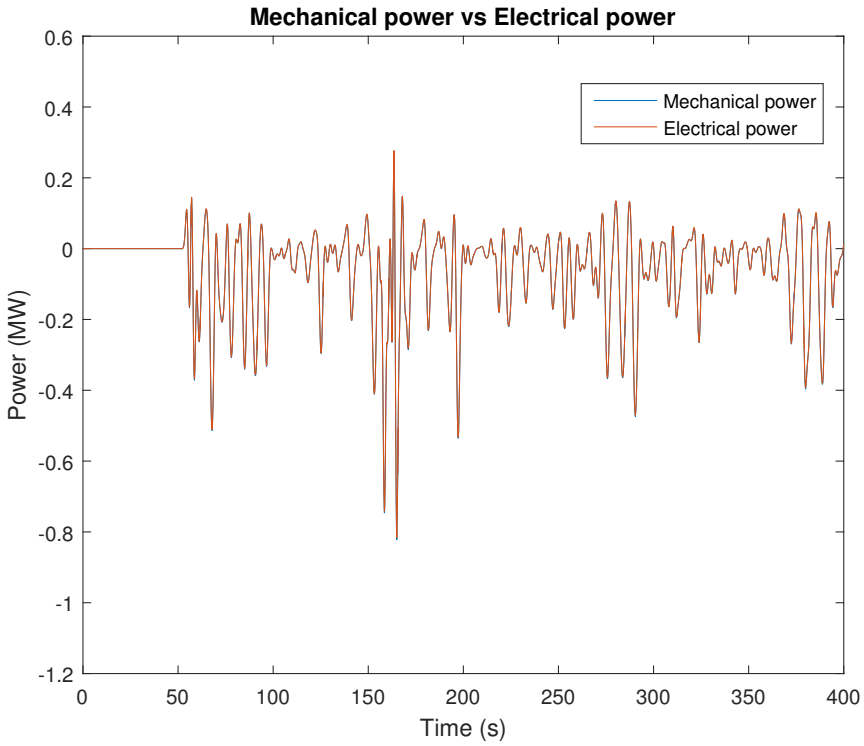

Figure 4.24: Electrical and mechanical power for integrated AC generator model (constrained)

In this case, the electrical efficiency was close to 98.5%. Like the previous case, it becomes difficult to control the system and hence the penalty matrix had to be tuned accordingly.

Chapter 5: Conclusion and future work

In conclusion, although the integrated PTO formulation seems to be viable, the following questions raised in chapter one were answered.

- Will the problem be convex?

  Initially, even without the generator model integrated into the system, the problem was slightly non-convex. However, adding a generator model seemed to make the problem even more non convex and meant more cost for control action which indicates an increase in cost for the power electronics.

- Will combining the generator model into the MPC formulation be feasible?

  The formulation for rate of change of current as control inputs for the integrated PTO model is definitely feasible especially for small scale WECs. However, precise tuning of the cost matrices are required as the amount of power captured is directly tied down to penalty for control action.

- How will this impact the efficiency & stability of the system?

  In terms of efficiency and stability, the rate of change of current formulation seems to be far more efficient and stable at low values at winding resistances which wasn't the case when the system was modeled with voltages as the control inputs. This was shown by observing the surface plots for winding resistances, emf constants and eigen values.

Future work could include a piece-wise linearization approach where the linearization points are updated at every time step based on the states. This would however lead to the coefficient matrices being re-built at every time step before running the optimization algorithm.

Bibliography

[1] Institute for Energy research. Renewable energy. Renewable-Energy, 2016. Accessed May 3rd 2017.

[2] EIA. United states energy facts explained. US Energy facts, 2016. Accessed May 3, 2017.

[3] Renewable Portfolio Standards. Renewable portfolio standard. Why Wave Energy?, 2016. Accessed May 3, 2017.

[4] Renewable Energy NorthWest. Renewable energy northwest. Renewable Energy NorthWest, 2007. Accessed May 3, 2017.

[5] Columbia wave Power. Why wave energy. Why Wave Energy?, 2013. Accessed May 3, 2017.

[6] Carnegi wave. Why wave energy. Why Wave Energy?, 2015. Accessed May 3, 2017.

[7] T. K. A. Brekken, B. A. Batten, and E. A. Amon. From blue to green [ask the experts]. *IEEE Control Systems*, 31(5):18–24, Oct 2011. ISSN 1066-033X. doi: 10.1109/MCS.2011.941960.

[8] B. Zanuttigh G. Bevilacqua. Overtopping wave energy converters,general aspects and stage of development. Overtopping, 2011. Accessed May 3, 2017.

[9] Wave Dragon. Wave dragon working. Wave Dragon, 2005. Accessed May 3, 2017.

[10] Gareth Thomas. *The Theory Behind the Conversion of Ocean Wave Energy: a Review*, pages 41–91. Springer Berlin Heidelberg, Berlin, Heidelberg, 2008. ISBN 978-3-540-74895-3. doi: 10.1007/978-3-540-74895-3_3. URL http://dx.doi.org/10.1007/978-3-540-74895-3_3.

[11] J. Falnes. A review of wave-energy extraction. *Mar Struct, 20*, 31(5):185–201, 2007.

[12] E. Rusch. Catching a wave, powering an electrical grid? Catching a Wave, 2009. Accessed May 3, 2017.

[13] Amélie Têtu. *Power Take-Off Systems for WECs*, pages 203–220. Springer International Publishing, Cham, 2017. ISBN 978-3-319-39889-1. doi: 10.1007/978-3-319-39889-1_8. URL http://dx.doi.org/10.1007/978-3-319-39889-1_8.

[14] B Drew, A R Plummer, and M N Sahinkaya. A review of wave energy converter technology. *Proceedings of the Institution of Mechanical Engineers, Part A: Journal of Power and Energy*, 223(8):887–902, 2009. doi: 10.1243/09576509JPE782. URL http://dx.doi.org/10.1243/09576509JPE782.

[15] Yue Hong, Rafael Waters, Cecilia Boström, Mikael Eriksson, Jens Engström, and Mats Leijon. Review on electrical control strategies for wave energy converting systems. *Renewable and Sustainable Energy Reviews*, 31:329 – 342, 2014. ISSN 1364-0321. doi: https://doi.org/10.1016/j.rser.2013.11.053. URL http://www.sciencedirect.com/science/article/pii/S1364032113008022.

[16] K. Budal and J. Falnes. Optimum operation of improved wave-power converter. *Mar. Sci. Commun.; (United States)*, 3:2, Jan 1977.

[17] S H Salter, J R M Taylor, and N J Caldwell. Power conversion mechanisms for wave energy. *Proceedings of the Institution of Mechanical Engineers, Part M: Journal of Engineering for the Maritime Environment*, 216(1):1–27, 2002. doi: 10.1243/147509002320382103. URL http://dx.doi.org/10.1243/147509002320382103.

[18] J.A.M. Cretel, G. Lightbody, G.P. Thomas, and A.W. Lewis. Maximisation of energy capture by a wave-energy point absorber using model predictive control. *IFAC Proceedings Volumes*, 44(1):3714 – 3721, 2011. ISSN 1474-6670. doi: http://dx.doi.org/10.3182/20110828-6-IT-1002.03255. URL http://www.sciencedirect.com/science/article/pii/S1474667016441893.

[19] Jeremiah Pastor and Yucheng Liu. Power absorption modeling and optimization of a point absorbing wave energy converter using numerical method. Spring Damping for a buoy, 01 June 2014. Accessed May 5, 2017.

[20] H. Eidsmoen. On theory and simulation of heaving buoy wave energy converters with control. *Ph.D. thesis Norwegian University of Science and Technology, Trondheim (1996).*

[21] T. K. A. Brekken. On model predictive control for a point absorber wave energy converter. In *2011 IEEE Trondheim PowerTech*, pages 1–8, June 2011. doi: 10.1109/PTC.2011.6019367.

[22] F. Fusco and J. V. Ringwood. A study of the prediction requirements in real-time control of wave energy converters. *IEEE Transactions on Sustainable Energy*, 3(1):176–184, Jan 2012. ISSN 1949-3029. doi: 10.1109/TSTE.2011.2170226.

[23] Guang Li, George Weiss, Markus Mueller, Stuart Townley, and Mike R. Belmont. Wave energy converter control by wave prediction and dynamic programming. *Renewable Energy*, 48:392 – 403, 2012. ISSN 0960-1481. doi: https://doi.org/10.1016/j.renene.2012.05.003. URL http://www.sciencedirect.com/science/article/pii/S0960148112003163.

[24] M. Starrett, R. So, T. K. A. Brekken, and A. McCall. Increasing power capture from multibody wave energy conversion systems using model predictive control. In *2015 IEEE Conference on Technologies for Sustainability (SusTech)*, pages 20–26, July 2015. doi: 10.1109/SusTech.2015.7314316.

[25] M. Starrett, R. So, T. K. A. Brekken, and A. McCall. Development of a state space model for wave energy conversion systems. In *2015 IEEE Power Energy Society General Meeting*, pages 1–5, July 2015. doi: 10.1109/PESGM.2015.7285998.

[26] Rowell. Analysis and design of feedback control systems; state-space representation of lti systems. Rowell, 2002. Accessed May 7, 2017.

[27] Six degrees of freedom, 2017. URL https://en.wikipedia.org/wiki/Six_degrees_of_freedom. [Online; accessed 7th May 2017].

[28] J. Falnes. *Ocean waves and oscillating systems*. Cambridge University Press, 2002.

[29] Mohan Ned. *Vector Control of Permanent-Magnet Synchronous Motor Drives*, pages 143–156. John Wiley & Sons, Inc., Cham, 2017. ISBN 9781118910962. doi: 10.1002/9781118910962.ch10. URL http://dx.doi.org/10.1002/9781118910962.ch10.

[30] Permanent magnet synchronous motor, 2013. URL https://www.mathworks.com/help/physmod/sps/ref/permanentmagnetsynchronousmotor.html. [Online; accessed 7th May 2017].

[31] A.J Jordan. *Linearization of non-linear state equation*. Bulletin of the Polish Academy of Science. Technical Science 54(1), 63–73 (2006), 2006.

[32] Moan Torgeir Hals Jørgen, Falnes Johannes. Constrained optimal control of a heaving buoy wave-energy converter. *Journal of Offshore Mechanics and Arctic Engineering*, 322(10):891–921, 2010/11/03. doi: 10.1115/1.4001431. URL http://dx.doi.org/10.1115/1.4001431.

[33] *Fundamentals of Unconstrained Optimization*, pages 10–29. Springer New York, New York, NY, 2006. ISBN 978-0-387-40065-5. doi: 10.1007/978-0-387-40065-5_2. URL http://dx.doi.org/10.1007/978-0-387-40065-5_2.

[34] J. V. Ringwood, G. Bacelli, and F. Fusco. Energy-maximizing control of wave-energy converters: The development of control system technology to optimize their operation. *IEEE Control Systems*, 34(5):30–55, Oct 2014. ISSN 1066-033X. doi: 10.1109/MCS.2014.2333253.